U. S. Army Communications-Electronics Command

Night Vision & Electronic Sensors Directorate

Title: Sensor Protection Portion of the Development of Nonlinear Optical Materials and Processes for Laser Hardening of Sensors

Author(s):
J. J. Song

Address: Center For Laser Research
413 Noble Research Center
Oklahoma State University, Stillwater OK 74078

Type of Report (Final, Interim, etc.):

Interim Final

Date: 10-31-94

Contract Number

DAAB07-88-C-F407

Report Number

NV-94-C11

Fort Belvoir, Virginia 22060-5806

SECURITY CLASSIFICATION OF THIS PAGE

REPORT DOCUMENTATION PAGE

Form Approved OMB No. 0704-0188

1a. REPORT SECURITY CLASSIFICATION: UNCLASSIFIED	1b. RESTRICTIVE MARKINGS: None
2a. SECURITY CLASSIFICATION AUTHORITY: N/A	3. DISTRIBUTION / AVAILABILITY OF REPORT: Approved for Public Release Distribution Unlimited
2b. DECLASSIFICATION / DOWNGRADING SCHEDULE: N/A	
4. PERFORMING ORGANIZATION REPORT NUMBER(S):	5. MONITORING ORGANIZATION REPORT NUMBER(S): NV-94-C11
6a. NAME OF PERFORMING ORGANIZATION: J. J. Song, Center For Laser Research; 6b. OFFICE SYMBOL (If applicable):	7a. NAME OF MONITORING ORGANIZATION: U.S. Army CECOM NVESD
6c. ADDRESS (City, State, and ZIP Code): 413 Noble Research Center, Oklahoma State University, Stillwater, OK 74078	7b. ADDRESS (City, State, and ZIP Code): 10221 Burbeck Rd.. Suite 430, Ft. Belvoir, VA 22060-5806
8a. NAME OF FUNDING / SPONSORING ORGANIZATION: ARPA; 8b. OFFICE SYMBOL (If applicable):	9. PROCUREMENT INSTRUMENT IDENTIFICATION NUMBER: DAAB07-88-C-F407
8c. ADDRESS (City, State, and ZIP Code): 3701 N. Fairfax Dr., Arlington, VA 22203-1714	10. SOURCE OF FUNDING NUMBERS: PROGRAM ELEMENT NO. 62 301 E; PROJECT NO.; TASK NO. DO; WORK UNIT ACCESSION NO.

11. TITLE (Include Security Classification): SENSOR PROTECTION PORTION OF THE DEVELOPMENT OF NONLINEAR OPTICAL MATERIALS AND PROCESSES FOR LASER HARDENING OF SENSORS.

12. PERSONAL AUTHOR(S): J. J. Song

13a. TYPE OF REPORT	13b. TIME COVERED	14. DATE OF REPORT (Year, Month, Day)	15. PAGE COUNT
Interim Final	FROM 92-1-1 TO 93-3-31	94-10-31	64

16. SUPPLEMENTARY NOTATION

17. COSATI CODES			18. SUBJECT TERMS (Continue on reverse if necessary and identify by block number)
FIELD	GROUP	SUB-GROUP	
20	5		
20	6		

19. ABSTRACT (Continue on reverse if necessary and identify by block number)

Nonlinear optical properties of several lead galliate glasses, CdMnTe and CdMnSe semiconductors, and SBN photorefractive crystals were studied in nanosecond and picosecond time regimes. Optical limiting characteristics of lead galliates were investigated as a function of the material properties, device geometeries and incident wavelengths. Broad band clamping was observed under nanosecond illumination. Nonlinear absorption and refraction in semiconductors were studied in the picosecond time regimes. A saturation in the nonlinear refraction at high input intensities were observed which may hinder applicability of these materials as picosecond optical limiters. Picosecond and subpicosecond photorefractive properties of SBN crystals revealed that in addition to the photorefractive behavior, this material exhibited induced absorption by retrapped pump generated carriers.

20. DISTRIBUTION / AVAILABILITY OF ABSTRACT	21. ABSTRACT SECURITY CLASSIFICATION	
☒ UNCLASSIFIED/UNLIMITED ☐ SAME AS RPT. ☐ DTIC USERS	U	
22a. NAME OF RESPONSIBLE INDIVIDUAL: Byong H. Ahn	22b. TELEPHONE (Include Area Code): (703) 704-2031	22c. OFFICE SYMBOL: AMSEL-RD-NV-LPD

"Interim Final Report"

SENSOR PROTECTION PORTION OF THE DEVELOPMENT OF NONLINEAR OPTICAL MATERIALS AND PROCESSES FOR LASER HARDENING OF SENSORS

Dr. Jin-Joo Song, Principal Investigator
Contract No. DAAB07-88-C-F407
Project No. ARPA Order No. 6324

Submitted to:
Byong H. Ahn
NVESD, LPD
10221 Burbeck Rd., Suite 430
Ft. Belvoir, VA 22060-5806

For Period: 1-1-92 through 3-31-93

TABLE OF CONTENTS

EXECUTIVE SUMMARY 2

1. INTRODUCTION 3

2. OPTICAL LIMITING IN LEAD GALLIATE GLASSES 7

    2.1. Introduction 7
    2.2. Experiment 10
    2.3. Discussion 12
        2.3.1. Device Parameters 12
        2.3.2. Material Parameters 16
    2.4. Conclusions 22

3. NONLINEAR OPTICAL AND TRANSPORT PROPERTIES OF CdMnSe and CdMnTe 24

    3.1. Introduction 24
    3.2. Nonlinear Optical Properties 25
    3.3. Carrier Dynamics 31
    3.4. Summary 35

4. NONLINEAR OPTICAL RESPONSE OF SBN 38

    4.1. Introduction 38
    4.2. Experiment 39
        4.2.1. Two Photon Absorption 42
        4.2.2. FWM: Experimental Results 46
            4.2.2.1. Picosecond-pulse excitation 46
            4.2.2.2. Subpicosecond-pulsed excitation 49
        4.2.3. Discussion 52
            4.2.3.1. Undoped sample 52
            4.2.3.2. Fe-doped sample 54
    4.3. Conclusions 57

5. SUMMARY AND RECOMMENDATION 58

6. REFERENCES 61

7. PUBLICATIONS 63

EXECUTIVE SUMMARY

The goal of our research was to identify suitable materials for optical limiting. During the first part of the project using a confocal geometry, experiments were performed on several different classes of materials. Thermo-optic effects in glasses showed the greatest potential. In this case, single and two photon absorption of light lead to local thermal changes which resulted in the attenuation of the index of refraction and absorption coefficient. These changes served to limit the transmitted light through an aperture via external self action. To determine the best glasses for optical limiting, experiments were performed to study the effects of the network former and modifier ions on the thermo-optic coefficient. These experiments indicated that glasses with a random network structure and containing lead as a modifier ion have the greatest thermo-optic coefficient. Among these, lead galliate showed the lowest clamping level (clamped transmitted energy / focal area at the 1/e height of a Gaussian beam in the material) of 52 mJ/cm^2 in an F/20 geometry using 7 ns pulses at 457 nm.

Using the desired F/5 configuration, optical limiting in lead galliate glasses was studied at various wavelengths for different glass compositions. A flat beam profile was used to better simulate the field circumstance of the device. Optical limiting was achieved for all the wavelengths used in the 440-640 nm range, with both on- and off-axis illumination. The clamping levels were lower for wavelengths with greater absorption. For example, a clamping level of 10 mJ/cm^2 at 457 nm for 7 ns pulses was accompanied with a linear transmission of 10%. Larger linear transmission resulted in higher clamping levels. A greater clamping level was also observed for off-axis beams. This was attributed to the focal plane curvature which may be corrected by proper lens design. Experiments performed on a variety of glass compositions and growth techniques showed similar clamping levels for lead galliate, lead gallio-silicate and lead gallio-germanate and small variation in the clamping levels for different growth techniques.

In an attempt to expand the time response of limiters to picosecond time regimes, a number of semiconductors and photorefractive materials were studied. The results of pump-probe experiments on CdMnSe and CdMnTe indicate that nonlinear refraction due to the free carriers is concentration dependent. This means that these materials may not be suitable nonlinear media in the high intensity regimes. Furthermore, broad band operation through two photon absorption is not feasible due to high threshold intensities needed. Introduction of defects may allow single photon absorption by the limited traps available but reduces the spectral width of device response. Similar results were obtained in strontium barium niobate (SBN) and SBN:Fe. Even though these materials exhibit a large photorefractive behavior, carrier generation via single photon absorption is narrow band and inefficient for the nonlinearities needed.

In conclusion, we have determined that glasses are still best suited material for optical limiting. In addition to their low production cost and durability, they demonstrate broad band optical limiting due to their broad absorption spectra. Perhaps by introduction of other dopants such as C_{60}, it will be possible to achieve a more constant optical limiting behavior throughout the visible spectrum and expand to different time regimes. Proper choice of other hosts may result in higher transmission for the same clamping levels.

1. INTRODUCTION

At the end of last year we completed our efforts on the sensor protection portion of contract number DAAB07-88-C-F407, project number:ARPA Order No.6324. The goal of the original proposal was to determine the feasibility of optical limiting for sensor protection. For this, we proposed to examine materials and geometries that may lead to the desired effect with the required specifications. After examining different materials (semiconductors, glasses, polymers) in geometries ranging from four wave mixing to self defocusing, we determined that optical limiting via thermal lensing had the greatest potential. Using a confocal geometry we were able to obtain clamping levels of a few mJ/cm^2 in lead based glasses. To maximize the thermo-optic behavior in these materials, optical limiting experiments were performed on several lead silicate, germanate, borate and phosphate glasses. From these experiments we concluded that:

1. The main contribution to the thermo-optic coefficient comes from the thermally induced changes in the electronic polarizability of the glass components and this is dominated by the contribution of the oxygen ions.
2. The thermo-optic coefficient is affected by the polarizing power of the network former ions.
3. Glass Networks with random structures have greater thermo-optic coefficients than the more rigid ring or chain structures.
4. The greatest influence of the network modifier ions is due to their effect on the absorption coefficient of the glass.

The purpose of the sensor protection portion was to complete the original work on this contract and extend the finding to different time regimes. For nanosecond optical limiting we focused on lead galliate glasses. In preliminary results, a clamping level of 52 mJ/cm^2 in an F/20 geometry was obtained for these glasses. During the extension period, we studied the limiting behavior of a number of lead galliate, gallio-silicate and gallio-germanate glasses in an F/5 geometry. This work included the study of the material parameters such as inclusion of other network formers and geometric parameters such as off-axis optical limiting. The work was done in collaboration with J. M. Jewell and J. Frieble of the Naval Research Laboratory who provided us with the glasses. The results of this study showed that:

1. Nanosecond optical limiting in these glasses was obtained through thermal lensing with presence of linear and nonlinear absorption.
2. Similar clamping levels were obtained for lead galliate, lead gallio-silicate and lead gallio-germanate. Furthermore, the SiO_2 concentration does not have any effect on the optical limiting behavior. Therefore, limiting is primarily dictated by lead oxide and gallium oxide components.
3. Alteration of the input beam profile from a radially varying function to a uniform top hat profile will not preclude optical limiting in these glasses.
4. Optical limiting can also be achieved for off-axis beams even though the optimum sample position is altered by the shift in the focal plane of the focusing lens.

To extend the work into picosecond and femtosecond time scales we looked at the nonlinear optical properties of several materials in these time regimes. Since optical nonlinearities due to thermal effects are negligible in pico- and femtosecond times, focus was

placed on semiconductors and photorefractive crystals. Particularly, we looked at nonlinear optical properties of dilute magnetic semiconductors (DMS) and strontium barium niobate (SBN) crystals.

In semiconductors, large optical nonlinearities are possible in the presence of free carriers. We studied the nonlinear optical properties and carrier dynamics of a number of CdMnTe and CdMnSe samples. The advantage of these materials over some other conventional semiconductors is their continuous band gap dependence on Mn concentration. Pump-probe experiments showed:

1. Two photon generated free carriers are the dominant contributing factor to optical nonlinearities in semiconductors.
2. The contribution of the free electrons to self-induced index changes varies with material composition as well as the band gap of the semiconductors.
3. The free carrier absorption is an important mechanism of beam depletion at input intensities of a few GW/cm^2.
4. At high carrier concentration, a saturation in the nonlinear refraction coefficient of the free electrons is observed which is associated with the increase in the effective mass of the higher laying electrons in the conduction band.

Finally, we looked at photorefractive behavior of undoped and iron doped SBN crystal in picosecond and femtosecond time regimes. Using laser induced grating technique, it was concluded that:

1. These materials possess a very large electro-optic coefficient. This makes the material suitable for optical limiting through beam fanning and other beam coupling techniques.

2. The photorefractive behavior is greatly enhanced with the additional of Fe to the SBN crystals even though iron doping did not affect the two photon absorption coefficient.
3. The crystals exhibit an induced absorption due to the retrapping of the pump beam generated free carriers.

The following sections expand on the observations outlined above in each of the materials studied.

2. OPTICAL LIMITING IN LEAD GALLIATE GLASSES

2.1. INTRODUCTION

The theoretical[1-5] and experimental[6-10] aspects of thermal lensing have been extensively studied. Recent investigations have shown that the effect can be utilized for optical limiting of laser pulses with duration in the nanosecond regime[11-14]. In materials with low thermal conductivities, the heat generated via absorption of laser excitation is confined to the region where it was generated. This local heating of the optical medium causes both expansion and change in the index of refraction, thus altering the optical path length. The medium now behaves as a lens, either focusing or defocusing the laser beam depending upon the radial profile of the change in the optical path length.

The theory of thermally induced refractive index changes has been discussed extensively. Here we give a brief overview of the generally accepted approach. For more detailed analysis, see Refs. 3, 4, 11-14. The refractive index of a medium including nonlinear effects is written as

$$n = n_o + \Delta n = n_o + n_2 I \qquad [2.1]$$

where n_o is the initial index of refraction, Δn is the change in the index of refraction, n_2 is the nonlinear refractive index and I is the intensity of the optical field. n_2 has many contributions such as Kerr, electrostrictive and thermal effects. In optical glasses exhibiting absorption, the thermal contribution to n_2 is the dominant contribution when the optical field is a laser pulse of nanosecond duration[9,13-15]. In this case we can write

$$\Delta n = \frac{dn}{dT}\Delta T \qquad [2.2]$$

where dn/dT is the thermo-optic coefficient and ΔT is the change in local temperature. It can be shown that n_2 is given by[3,4,13,14]

$$n_2 = \frac{\alpha\tau}{\rho c}\frac{dn}{dT} \qquad [2.3]$$

where α is the absorption coefficient (including nonlinear absorption if present), ρ is the density and c is the specific heat of the glass and τ is the pulse width (square pulse) of the optical field.

A number of material parameters will influence the performance of a thermal lens based passive optical limiter. For strong thermal lensing, larger local heating and slower diffusion are needed. Also, low density and small specific heat are desirable to increase n_2 (Eq. (2.3)). Although a large absorption coefficient enhances n_2, a practical optical limiter should have low absorption loss in the linear regime. Thus, the absorption coefficient must be balanced to provide sufficient heat generation for an effective thermal lens at high intensities, but provide adequate transmission at low intensities. The size and sign of the thermo-optic coefficient dn/dT is also very important. It has been found that optical limiters designed with materials having a positive dn/dT perform better than those with materials having a negative dn/dT of the same magnitude[13-16]. A positive value of dn/dT leads to self-focusing of the incident beam while a negative value leads to self-defocusing. The effects of self-focusing are enhanced as the beam propagates through a medium while the effects of self-defocusing are reduced upon propagation into the medium because of the reduction in intensity. The passive optical limiter described in this work consists of a simple telescope with a material exhibiting thermal lensing placed near the intermediate focal plane (Fig. 2.1). For either positive or negative dn/dT the

area of the beam at the second aperture can be made *larger* than it would be with no material present by a suitable choice of the sample position in the system and limiting will result.

In this section we describe some of the results of our continuing investigation of a passive optical limiter using thermal lensing in lead based glasses. Glasses incorporating lead as a modifier ion were previously found to exhibit reasonable optical limiting[13]. That work concentrated on determining the effect of glass structure and composition of performance. Here we investigate a relatively new glass system, the lead galliate system[17,18] and again investigate some of the effects of composition on optical limiting performance. The compositions used are given in Table 2.1. Effects associated with incorporating additional network formers are considered. The results are compared with and interpreted in terms of those found in the previous study. The effects of changes in the glass preparation conditions are also investigated. Further, effects independent of material properties but associated with the overall device geometry and performance are also considered.

Table 2.1. Glass Composition

Glass	Label	Composition (mol%)					Thickness (mm)
Lead Galliate		PbO	Ga_2O_3				
	LG1	70	30				1.45
					Crucible	Atmosphere	
	LG2	75	25		Pt	air	1.29
	LG3	75	25		Pt	oxygen	1.50
	LG4	75	25		Au	air	1.45
Lead Galliate	LGB	PbO	Ga_2O_3	B_2O_3			
Borate		60	25	15			3.45
Lead Galliate	LGG	PbO	Ga_2O_3	GeO_2			
Germanate		60	25	15			2.25
Lead Galliate	LGS	PbO	Ga_2O_3	SiO_2			
Silicate		60	25	15			3.25

2.2. EXPERIMENT

The experimental set up used in this investigation is shown in Fig. 2.1. A nitrogen laser pumped dye laser providing 7 ns pulses operating at 10 Hz was used. The dye laser was tunable throughout the visible spectral range with a choice of suitable dyes. The optical limiting configuration used was that of an intermediate focal plane device with fixed aperture diameters. The first lens focused light onto the sample while the second lens was used to recollimate the transmitted light. The second lens was adjusted with no sample in the device such that the output beam was collimated and had the same diameter as the incident beam. Overall transmittance without a sample was 85% of the incident energy. Both apertures had the same diameter and both lenses had the same focal length. The diameter and focal length were chosen so that the F-number of the system was F/5. A dual probe energy meter triggered with a photo diode was used to monitor the incident and transmitted energies. A beam splitter was used to split off part of the incident pulse and direct it to one of the probes that was calibrated to the energy incident on the sample. The incident beam was expanded in diameter to deliberately over fill the entrance aperture to produce a flat field intensity profile.

Optical damage was incurred from both single shot and cumulative exposure. The mechanism and effects of this damage are extremely complex and are beyond the present discussion. To avoid the effects of cumulative exposure, the sample was translated in the *x-y* plane between pulses to provide a fresh location. All the experimental results reported here were obtained by illuminating a given sample location with only a single laser pulse selected from the 10 Hz pulse train by a mechanical shutter.

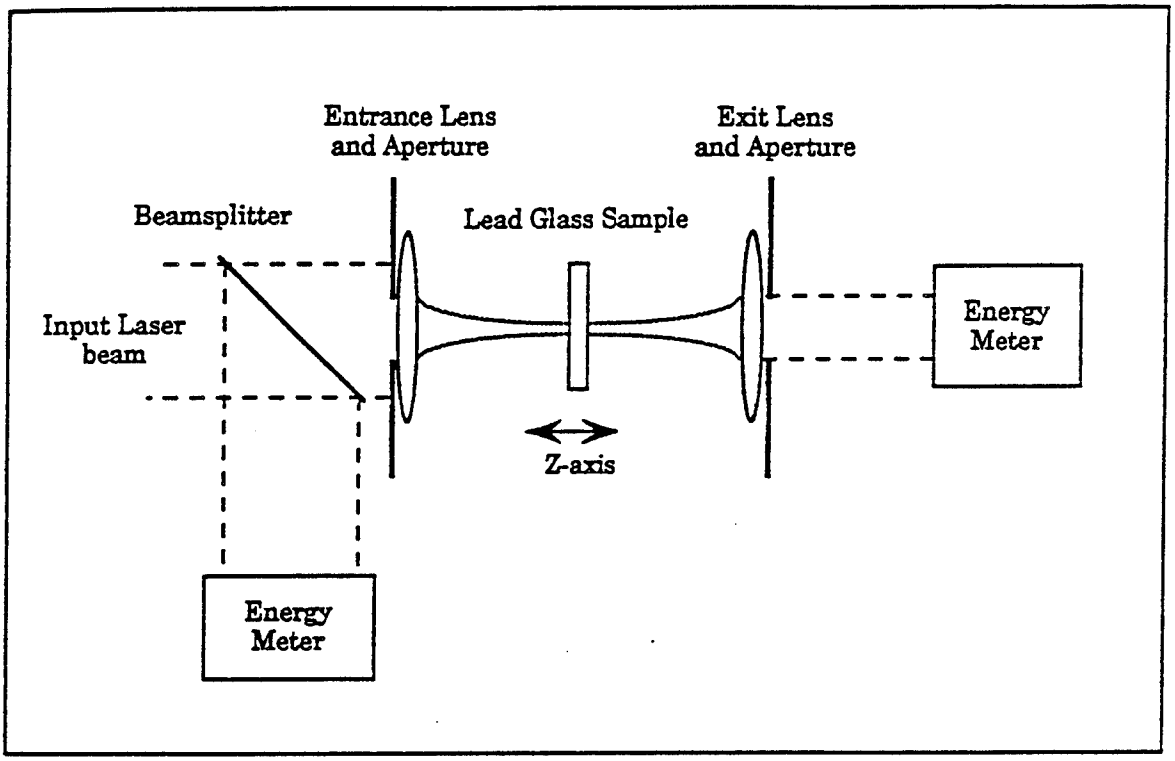

Fig. 2.1. Experimental setup for Z-scan and optical limiting. The focal length/ aperture diameters used were 16.0 mm/ 3.2 mm to give an F/5 optical system.

Two types of experiments were performed on the samples. The first experiment in all cases was a Z-scan. In this experiment the position of the sample along the optic axis (Z-axis) of the system was varied while being illuminated with a constant (10%) incident energy. The energy transmitted through the second aperture was collected by the energy meter and the optimum sample position for limiting (the position with the lowest transmitted energy) was determined; then a fluence transmission (FT) experiment was performed. With the sample at a fixed Z position, the incident energy was varied and the transmitted energy recorded. Because of the wide spectral range investigated and to preserve the spatial homogeneity of the beam profile, neutral density filters rather than waveplate/polarizer combinations were used to attenuate the laser pulses.

2.3. DISCUSSION

2.3.1. Device Parameters

The results in Fig. 2.2 show the typical behavior seen for nearly all the samples investigated here. It should be noted that the input fluence is defined as the input energy divided by the beam area prior to the focusing lens and the output fluence as the transmitted energy divided by the beam area at the focus. The Z-scan experiment (Fig 2.2(a)) shows a transmission minimum indicating significant optical limiting. Similar results to these have been reported previously in oxide glasses[13,14]. Note that there are no peaks observed here in the Z-scan data as reported in other materials[16-19] because the exit aperture diameter was matched to the undisturbed laser beam diameter. In a closed aperture Z-scan, where the aperture is set less than the undisturbed beam diameter, the lack of a significant peak in the Z-scan is interpreted as evidence of nonlinear absorption contributing to the limiting[13,14]. Fluence transmission data

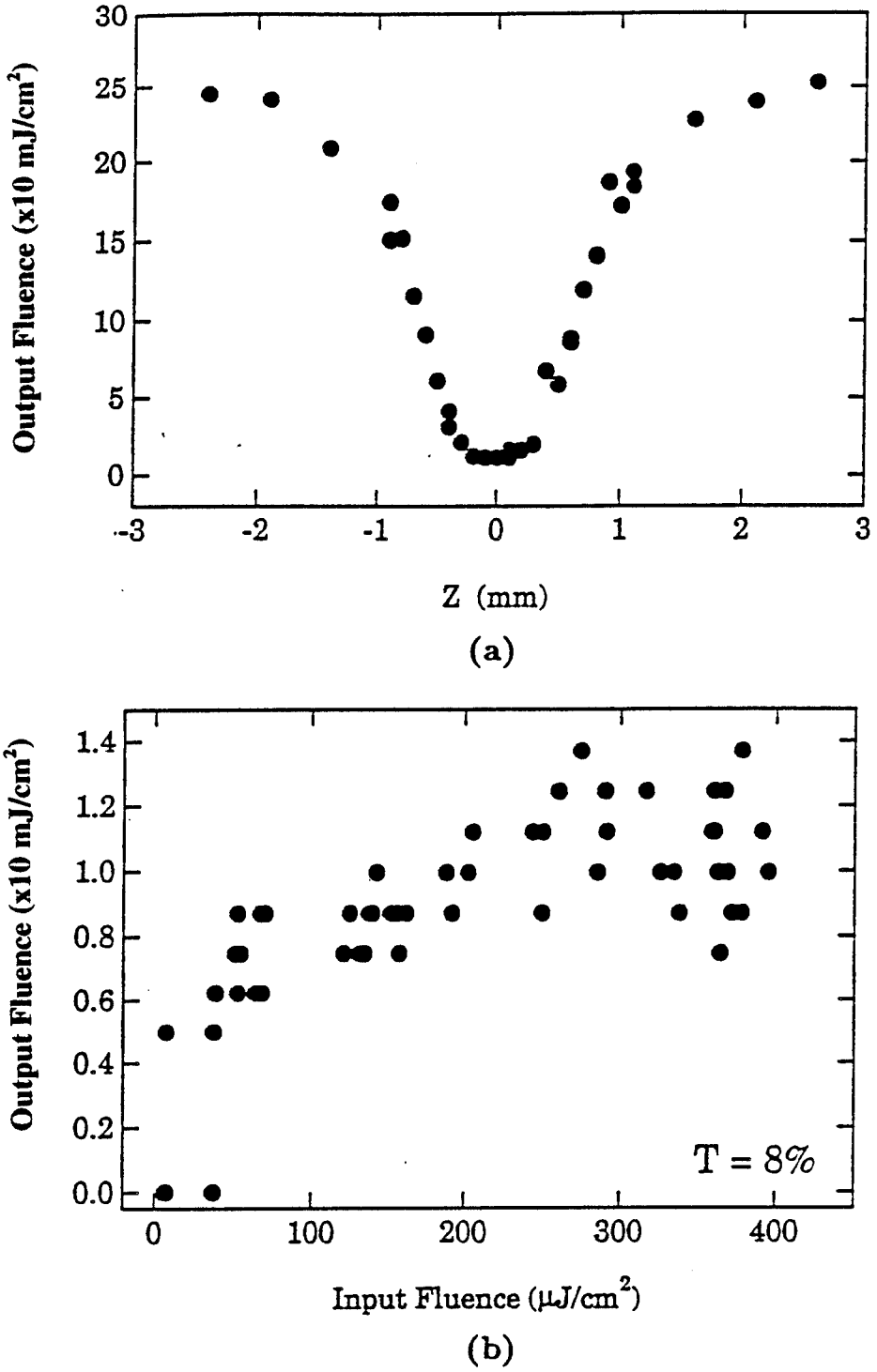

Fig. 2.2. Typical results of (a) Z-scan and (b) optical limiting experiments at a wavelength of 457 nm. The glass used was 70% PbO, 30% Ga_2O_3.

(Fig 2.2(b)) demonstrate typical limiting behavior at high intensities and show a significant deviation from linear transmission even at the lowest intensities measured. Effective optical densities ($\log(I_T / I_o)$) greater than 2 have been induced.

From a purely engineering point of view, an important aspect of the limiting results is that they were obtained with a nearly uniform spatial beam profile after the entrance aperture. Figure 2.3(a) shows the spatial profile of the transmitted beam just after the second lens without a limiting sample. Here the second aperture had been removed and a 2-dimensional detector was placed a few cm from the second lens. With the LG1 sample in place at its optimum Z position, there is clearly an optically induced increase in the beam area (Fig. 2.3(b)). This plot was recorded with a single laser pulse of input fluence 700 $\mu J/cm^2$ and wavelength of 590 nm. Thus, one mode of limiting of the glass can clearly be seen since with the second aperture in place, part of the output beam is blocked and the overall transmission is reduced. This beam fanning is an indication of lensing effect arising from refractive index changes in the sample due to both linear and nonlinear absorption induced local heating. Additionally, there will be depletion due to nonlinear absorptive effects. Since both self-focusing and self-defocusing effects in the material can lead to a larger beam diameter at the position of the second aperture, the sign of dn/dT cannot be determined from the spatial profile information alone. Previous results indicate that dn/dT is positive in material similar to those under study here[13,14]. It is useful to make a comparison with the new material under study here. The experiments show that when compared in the same optical system, the lead galliate glasses exhibit a clamping level nearly an order of magnitude lower than the lead silicates; that is, the galliates have an improved material performance. It is interesting to note that in absolute terms the lead galliate glasses

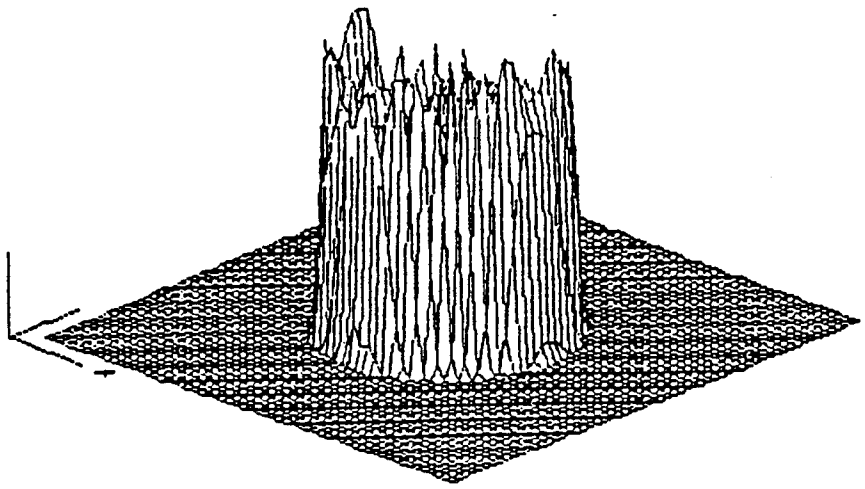

(a)

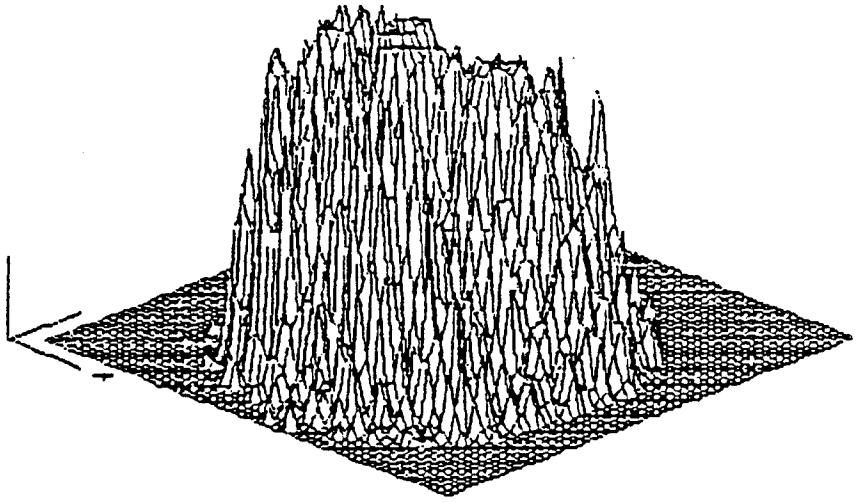

(b)

Fig. 2.3. Spatial profiles of the laser beams along the optic axis for the F/5 'flood loaded' system measured after the second lens and without the aperture: (a) without a sample, and (b) with 70% PbO, 30% Ga_2O_3 glass sample in optimum Z-position.

show a similar clamping level in the F/25 and F/5 optical systems. The input intensity in our earlier F/25 configuration had a nearly Gaussian radial profile. Since the refractive index change in the material follows the radial profile of the illumination, a larger radial variation in the refractive index produces a stronger lensing effect. The F/5 configuration has a smaller spot size at the sample that yields higher intensity, but as detailed earlier there is little variation in the spatial profile. Thus, it appears that similar clamping levels are obtained in the two optical systems because the increased intensity is offset by the more uniform radial distribution.

The use of a small F/# system also increases the field of view of the system. Therefore, in addition to on-axis illumination, off-axis angle becomes important. Figure 2.4 shows the results of FT experiments in the LG1 sample for beam propagation at several off-axis angles. These results, recorded with the optimum Z position determined for on-axis angles, show that the optical limiting performance had degraded significantly by the time an off-axis angle of 4.5 degrees is reached. It was found that the Z position for off-axis propagation had moved closer to the first lens. If the Z position is optimized for illumination at the off-axis angle, the optical limiting performance of the glass approached that of on-axis propagation. This movement of the optimum Z position is attributed to a change in position of the focal plane due to astigmatic aberrations in the simple lenses used.

2.3.2 Material Parameters

Figure 2.5 shows the wavelength dependence of the limiting behavior for the sample LG1. The optical limiting performance degrades at longer wavelengths following the decreasing linear absorption. However, even at wavelengths where there is little linear absorption the actual

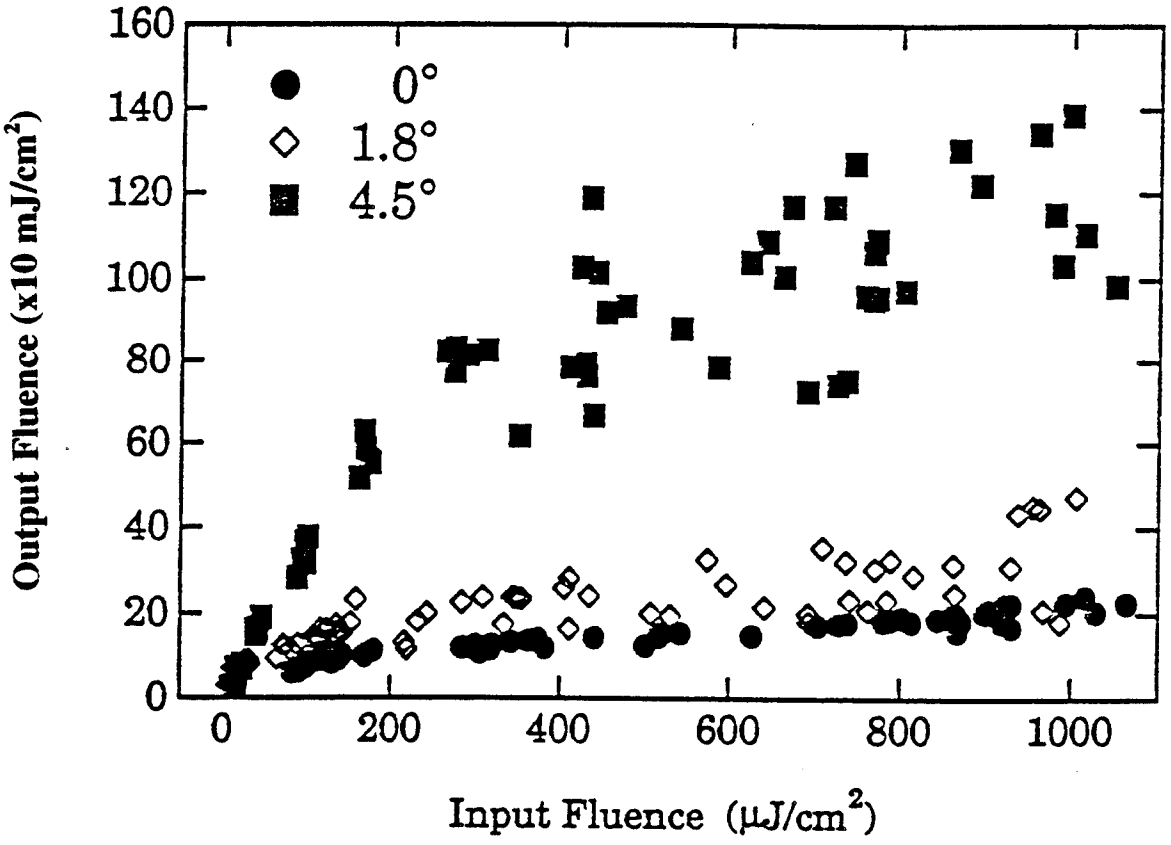

Fig. 2.4. The effects of off-axis propagation on optical limiting results. The optimum Z position was determined with on-axis illumination and limiting done off-axis at the angle indicated. The sample was a 70% PbO 30% Ga_2O_3.

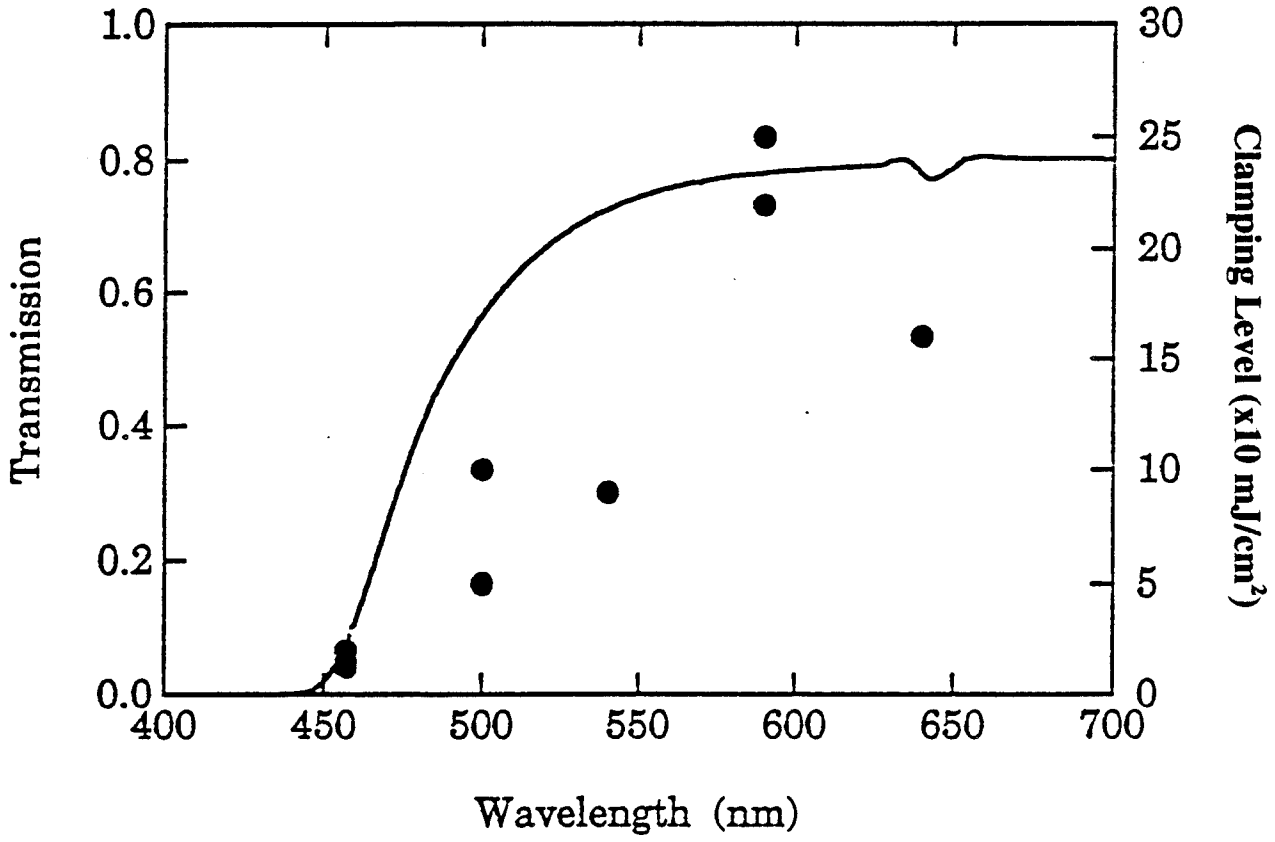

Fig. 2.5. Wavelength dependence of fluence transmission results for a 70% PbO 30% Ga_2O_3 glass. The solid line indicates the linear transmission spectra and the solid circles are the optical limiting results.

transmission at high intensities is very low and limiting occurs, most likely arising from nonlinear absorptive effects.

The effects of various network formers and the structure of glasses on optical limiting behavior were previously investigated[13,14]. A significant trend relating the structural nature of the glass (random *vs.* ring or chain structure) to limiting behavior was observed. Random networks, such as those in silicate or germanate glasses, performed better than ring-like networks, such as those found in borates and phosphates. Figures 2.6(a)-(c) show new FT results on the lead galliate based ternary systems. The results show all three systems exhibiting comparable limiting behavior. At the concentrations used the traditional network formers (SiO_2, GeO_2, and B_2O_3) play only a secondary role with the main structural properties determined by the other glass constituents, PbO and Ga_2O_3. Structural studies of the lead gallio-sillicate ternary indicate that at concentrations >25% of Ga_2O_3 the structure is dominated by [GaO_4]-tetrahedral units charge compensated by Pb^{2+} ions[20]. Additional SiO_2 participates in this tetrahedral network. Although structural studies of the germanate and borate analogous to the silicates are not available, the similar optical limiting results here indicate these typical network formers play similar non-dominant roles at these concentrations.

Finally, the effects of crucible material and melt atmosphere on limiting behavior were investigated. Three samples of 75% PbO-25% Ga_2O_3 glasses were produced using three different melt conditions (Table 2.1). A comparison of the results (Fig. 2.7) indicates differences in the transmission spectra of the glasses and different limiting levels. The use of a gold crucible shifts the absorption edge to shorter wavelengths and leads to an increase in the limiting level at shorter wavelengths. The use of an oxygen atmosphere during glass preparation

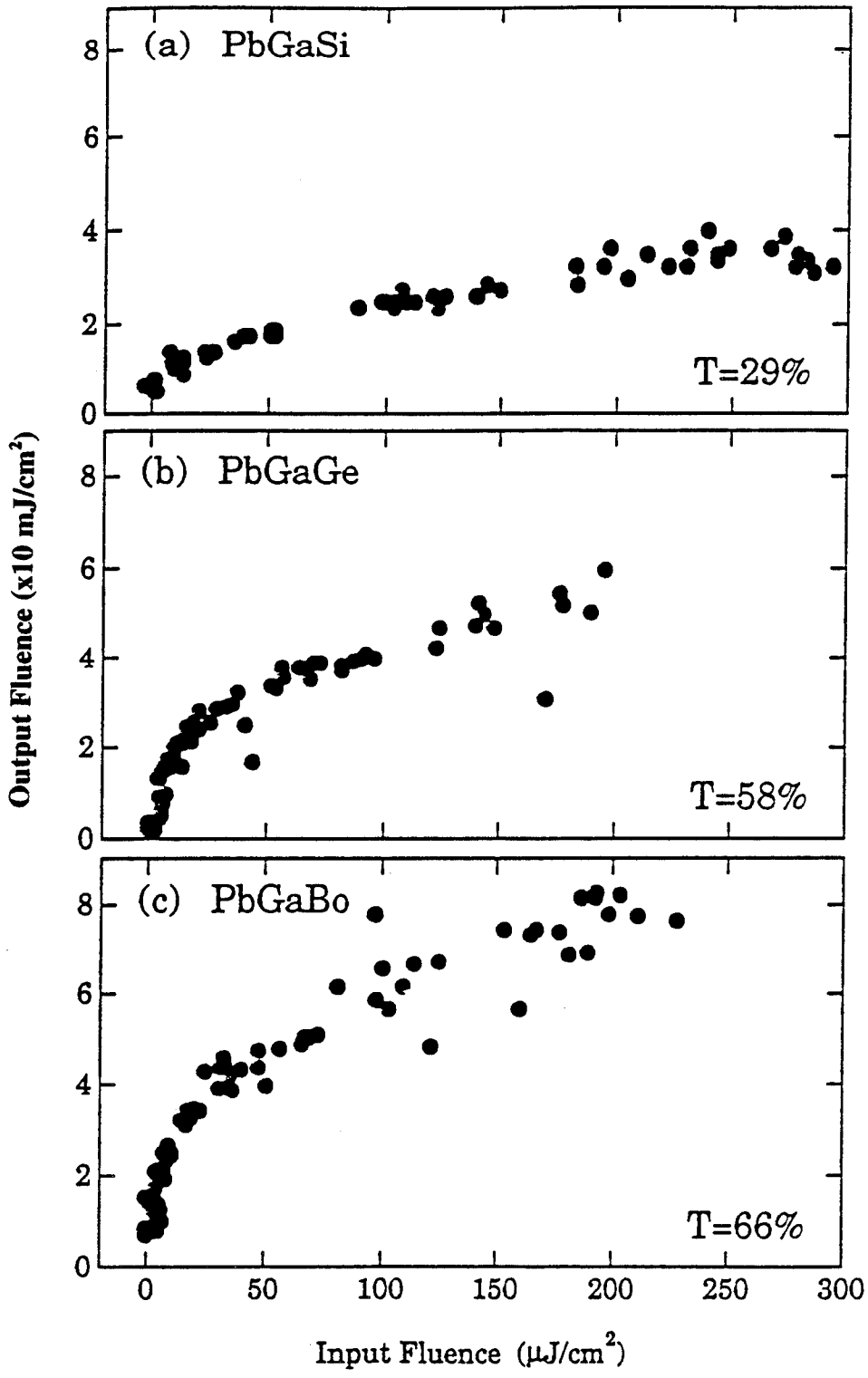

Fig. 2.6. Optical limiting results for samples containing various network formers in the lead galliate ternary system.

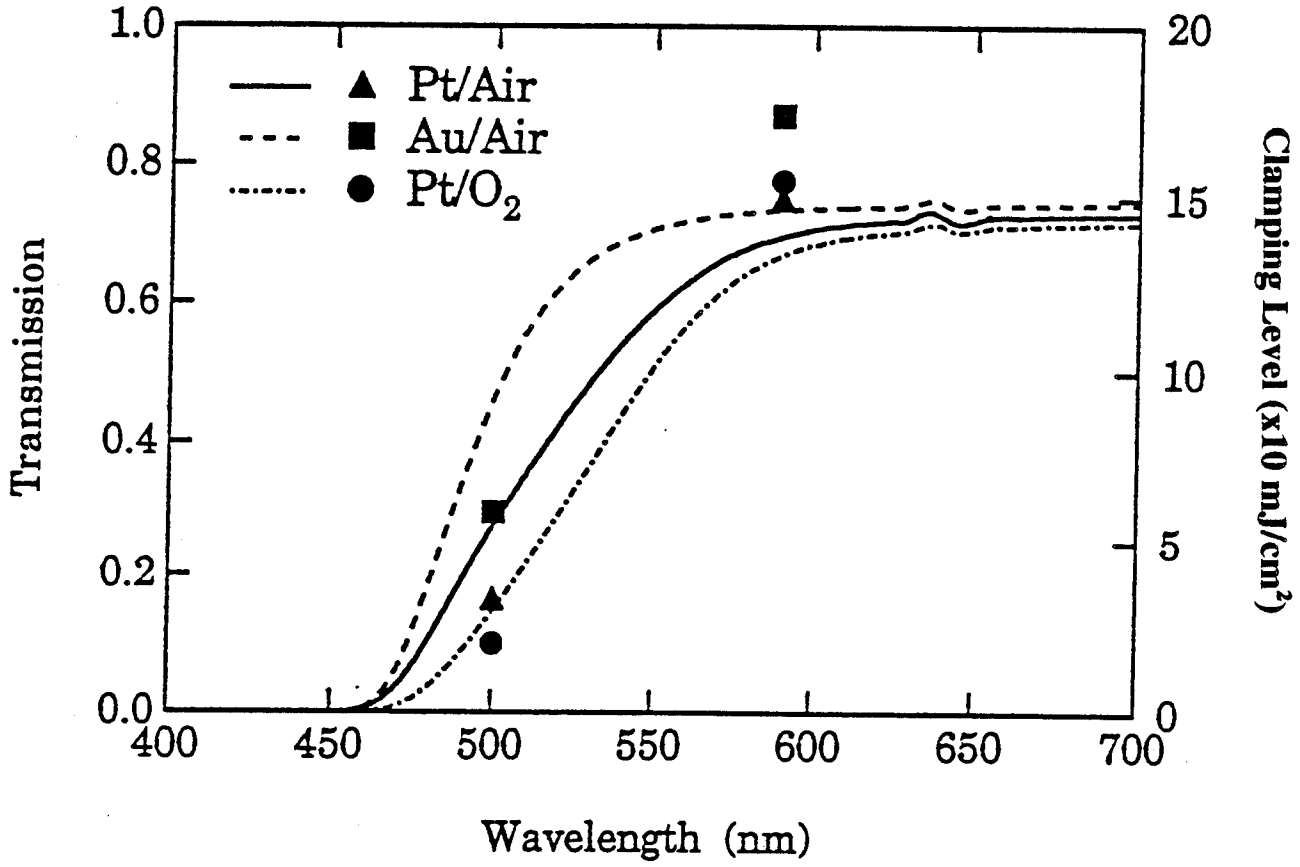

Fig. 2.7. Comparison of transmission and limiting behavior for 75% PbO 25% Ga_2O_3 glasses prepared with different crucible materials and melt atmospheres. Results for the two different wavelengths are shown. The lines indicate the linear transmission spectra and the symbols are the optical limiting results.

shifts the absorption edge to longer wavelengths, increasing the linear absorption and enhancing the thermal lensing effect. This leads to a decrease in the limiting level at shorter wavelengths.

2.4. CONCLUSIONS

Optical limiting has been observed and investigated in a new family of glasses: the lead galliate binary system and the ternary systems lead gallio-silicate, lead gallio-germanate, and lead gallio-borate. One of the mechanisms contributing to the optical limiting was identified as that of thermal lensing with both linear and nonlinear absorption mechanisms contributing. Limiting behavior of the various ternary systems was similar regardless which of the three traditional network formers was used as the third component. Altering the SiO_2 concentration within the lead gallio-silicate ternary did not modify limiting behavior significantly. These two results indicate that the limiting properties of these glasses are determined primarily by the lead oxide and gallium oxide components. Composition changes within the lead galliate binary also did not alter overall limiting behavior significantly. The change in structural properties at the 75% PbO-25% Ga_2O_3 composition observed previously[20] does not seem to significantly affect the optical limiting behavior.

Broad band operation of these materials was also demonstrated. Optical limiting was observed throughout the 440-640 nm spectral range investigated. The clamping level vs. wavelength trend seems to follow that of the linear transmission but further investigation of the details of this relationship need to be performed since limiting occurs at wavelengths where there is little linear absorption.

An important result of this work is that the results were obtained using a nearly uniformly illuminated F/5 optical system. The lack of a substantial variation in the radial beam

intensity did not preclude optical limiting. This is important for the further study of optical limiters for applications where the radial beam profile may vary. Additionally, the problems associated with off-axis illumination were demonstrated. The clamping behavior was found to be dependent on the procedure used to determine the optimum Z-position. For off-axis limiting the optimum Z-position was nearer the first lens than for the on-axis case which was attributed to a shift in the focal plane position for off-axis propagation. In the design and construction of a practical optical limiter, both device dependent and material dependent parameters, some of which have been examined, here need to consider.

3. Nonlinear Optical and Transport Properties of CdMnSe and CdMnTe

3.1 INTRODUCTION

II-VI semiconductors containing Mn belong to classification of the materials known as Diluted Magnetic Semiconductors (DMS). What sets these materials apart from other semiconductors containing transition metal ions is the large solubility of the Mn in the host. This leads to a continuous change in the lattice parameter and band gap of these materials [21,22]. The enhanced magneto-optical properties of these materials have been extensively studied and for the most part understood. Their nonlinear optical properties, however, are less known. With this in mind, experiments were performed to determine the nonlinear optical and carrier dynamics of $Cd_{1-x}Mn_xTe$ and $Cd_{1-x}Mn_xSe$ samples with several Mn concentrations.

The nonlinear optical properties of semiconductors can be categorized as those arising from the bound electrons and those due to free carriers. The nonlinearities due to the bound electrons are instantaneous and will follow the temporal shape of the pulse. In the case of the third order susceptibility tensor, these result in the two photon absorption, β, and the bound electron nonlinear refraction, γ, coefficients. To a good approximation, these parameters have shown to be material band gap dependent and their values have been estimated for a range of semiconductors[23,24]. Therefore, we shall focus on the effects of free carriers on the optical nonlinearities.

This section will be divided into two subsections; the first dealing with the nonlinear optical properties and the second with the carrier dynamics. The study was done using a mode-locked, Q-switched, Nd:YAG laser operating at 1064 nm with a FWHM of 27 ps.

3.2 NONLINEAR OPTICAL PROPERTIES

The photon energy at this wavelength is smaller than the band gap of the materials under investigation, and therefore free carrier generation takes place via two photon absorption. The generated carriers will then modulate the absorption coefficient and index of refraction of the material. Since these effects persist while the electrons remain in the conduction band, it is possible to monitor their effects after the excitation pulse has passed. If the number of generated carriers were known, it would be a relatively simple task to determine the changes induced by them. In particular, if the excitation pulse has a Gaussian intensity profile, the post sample spatial profile of a delayed probe beam can then be used to determine the effect of the carriers.

Figure 3.1 shows the experimental setup used to study the third order nonlinearities in our samples. The probe beam is delayed 100 ps from the pump beam to ensure that there are no interactions between the beams. Both beams are passed through a $1m$ focal length lens and have the same beam radius of 590 μm at the front surface of the sample. Each sample was placed 29cm behind the focal plane of the lens. The samples were 'thin' compared to the Rayleigh range of the beams (30 times smaller) to ensure applicability of the thin medium formalism [25]. The energy of the pump beam was varied by a waveplate-polarizer combination and that of the probe was kept fixed at a level where no self-induced optical nonlinearities were measurable. The apertures placed in front of the detectors are to monitor the total and the on-axis transmission of each beam. The detected energy at each meter was stored in a computer as a function of the input energy of the pump beam.

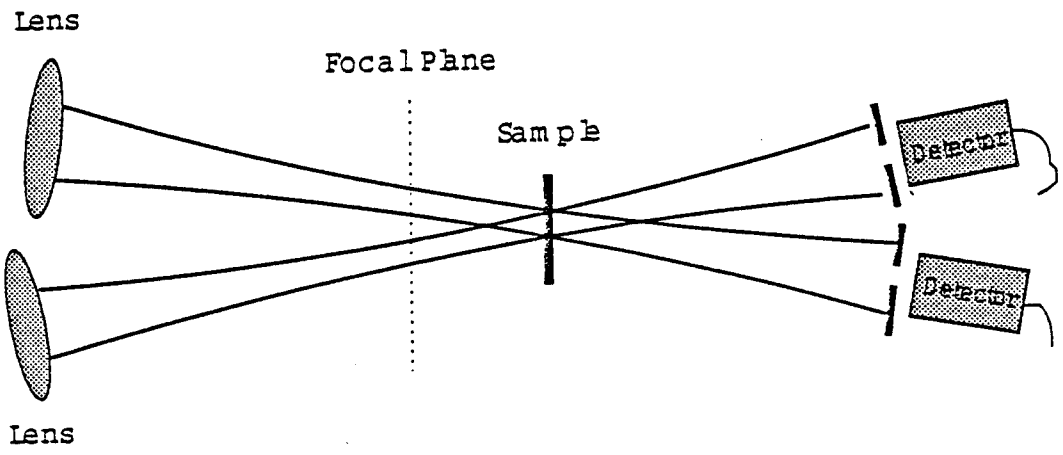

Fig. 3.1. Experimental setup for measuring the nonlinear optical properties.

The amplitude, I, and the phase changes, ϕ, of post sample incident pump beam are given by[23]:

$$\frac{dI}{dz} = -\alpha I - \beta I^2 - \sigma N \qquad [3.1]$$

and

$$\frac{d\phi}{dz} = k(\gamma I + \sigma_r N) \qquad [3.2]$$

where for the laser photon energies ($h\omega$ <Egap) the carrier concentration, N, is given by:

$$\frac{dN}{dt} = \beta \frac{I^2}{2h\omega} \qquad [3.3]$$

Here, k is the wave vector of the incident pump beam, α is the absorption coefficient of the material, σ is the free carrier absorption cross section, and σ_r is the nonlinear refraction coefficient of the free electrons. In Eq. 3.3 any recombination of the carriers is neglected since the lifetime of the carriers are much greater than the 27 ps pulsewidth of the laser. A similar set of equations can be used for the delayed probe beam. However, any changes of the probe beam amplitude and phase are a result of the pump beam generated free carriers. In terms of the above equation, this means contributions from the σN and $k\sigma_r N$ terms only. From Eq. 3.2 we see that the concavity of the induced absorptive lens is given by the sign of the phase change. In general, these coupled equations have to be solved numerically. The field at any plane past the sample can, then, be calculated by a zeroth order Hankel transform of the field at the exit plane[26].

Figures 3.2(a) and (b) show the transmission coefficients of the pump and probe beams obtained in a fully open aperture experiment performed on CdTe. In this case, changes in the phase front will not effect the results, and the changes in the transmission coefficients are solely due to the two photon and free carrier absorption coefficients. For the probe beam, these changes are a result of the free carrier absorption only. The lines in the graphs correspond to normalized transmission of the pump and probe beams for various values of β and σ values. The use of both graphs will uniquely determine each coefficient.

Figure 3.3 shows the normalized transmission coefficient of the probe beam obtained in a small aperture experiment performed on CdTe. Here, the relevant parameters for the probe beam are σ (which was determined earlier) and σ_r. Comparing the probe transmission in figures 3.3 and 3.2, we see that the probe transmission decreases more rapidly in the small

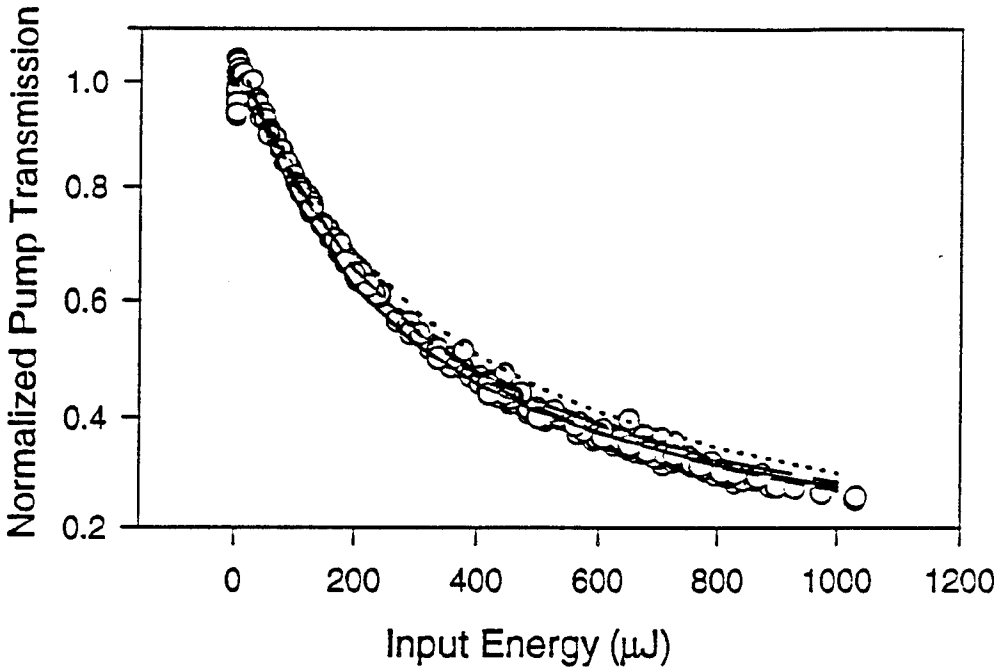

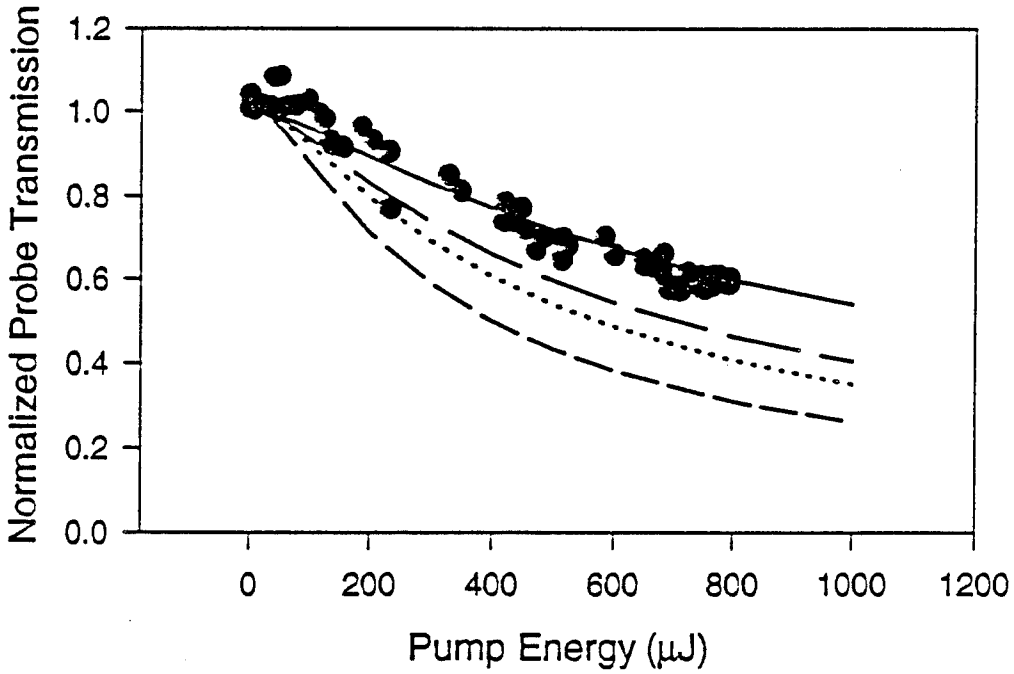

Fig.3.2. Results of the open aperture experiment on CdTe for (a) pump beam and (b) probe beam. The circles are the data points and the lines are the solution of Eqs. 3.1-3.3.

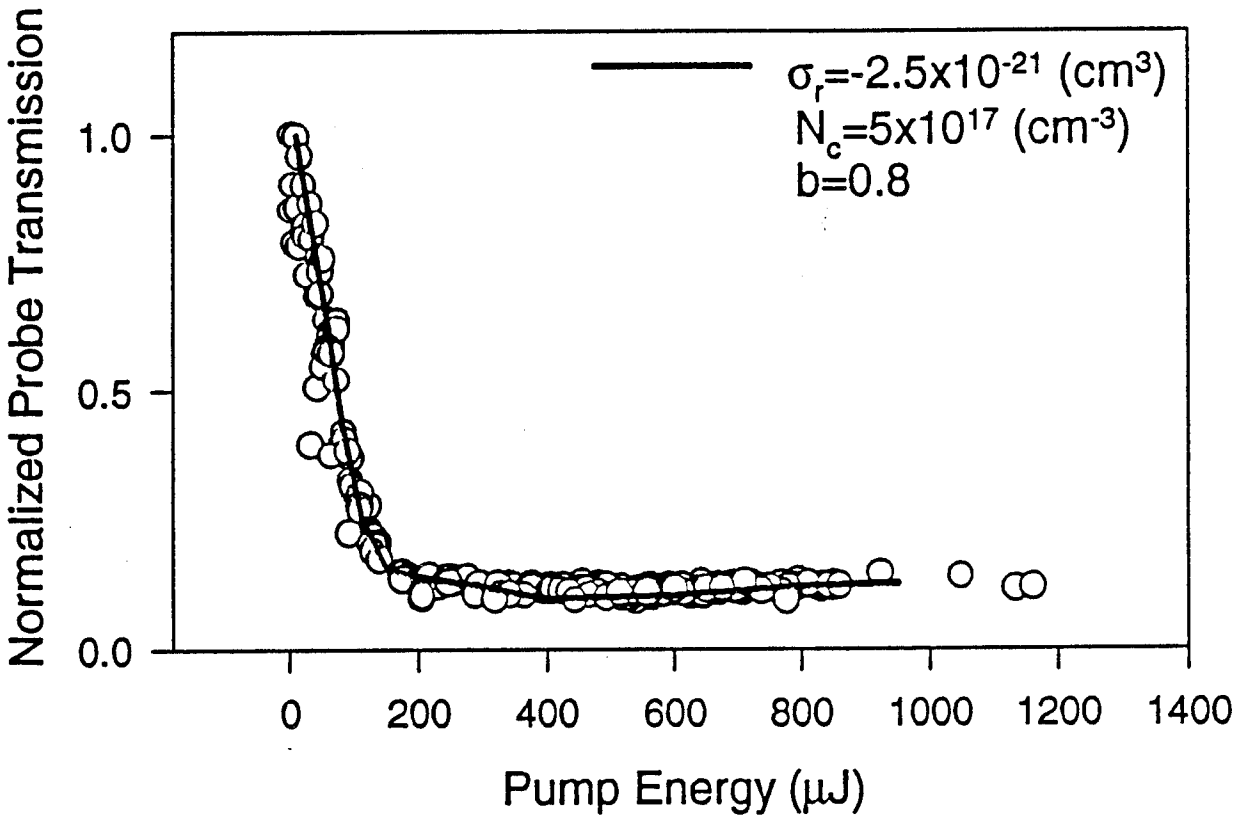

Fig. 3.3. Results of the closed aperture experiment on CdTe for the probe beam. The fit was obtained using Eq. 3.6 for σ_r.

aperture experiment than in the case of an open aperture experiment. This suggests that the free carrier induced lensing behaves as a negative lens. However, the sharp saturation in the transmission coefficient could not be described by Eq. 3.1-3.3. In particular, a fit could only be obtained if the value of σ_r were to decrease with an increase in the pump energy or, in other words, with carrier concentration. We believe that this is due to the dependence of the effective mass on the carrier concentration. This is to be expected since at high electron concentrations, states higher than the bottom of the conduction band are occupied. It has been shown that the effective mass of the electrons has an energy dependence given by[27]:

$$m^* = m_o^*\left(1+2\frac{E-E_c}{E_{gap}}\right) \qquad [3.4]$$

with $E\text{-}E_c \approx E_f$, where E_f is the Fermi energy. When carrier concentrations exceed a critical value, N_c, the quasi-Fermi level will be within the conduction band and thus the effective mass of the carriers will differ from the dilute case. In general, the location of the Fermi level with respect to the bottom of the band is dictated by the Fermi integral[28], but for our case it can be approximated by $E_f \sim a(\ln(N/Nc))^2$. This means that the effective mass of an electron is given by:

$$m^* = m_o^*(1+b(\ln(N/N_c))^2) \qquad [3.5]$$

which implies that:

$$\sigma_r = \begin{cases} \sigma_{ro} & for\ N < N_c \\ \sigma_{ro}/[1+b(\ln(N/N_c))^2 & for\ N \geq N_c \end{cases} \qquad [3.6]$$

Using the above, we noticed that the slope of the transmission coefficient for $N<N_c$ was dictated by σ_{ro}, and the saturation level was determined by b and N_c values. The values for *b* and N_c obtained using the fit correspond well to the expected values for these parameters.

3.3 CARRIER DYNAMICS

The decay of the nonlinear optical behavior described above is dictated by the electron recombination time and diffusion coefficient. To study these properties, we used a forward propagating laser induced grating technique. The probe beam was at an angle of 2 degrees to the plane of the pump beams. The scattered and the transmitted probe will, therefore, be out of the plane of the pump beams which allows for the detection of the total energy in them. The energy ratio between the two pump beams was kept at 1:1, and they were focused to a 1*mm* radius and crossed at the sample. The crossing angle for the two pump beams, 2θ, was 9.5° degrees, which corresponds to a grating spacing of 6.5 μm. The probe beam energy was kept constant and had a beam radius of 0.3mm at the sample. The smaller radius of the probe helps minimize any effects arising from the Gaussian nature of the pump beam spatial profile. The energy of the transmitted and the scattered probe beam was monitored by two LaserPrecision energy meters. This was done as a function of the pump beam energy and the probe beam delay.

The scattering efficiency, η, of a light, scattering from a sinusoidal grating is given by[29]:

$$\eta = e^{-(\alpha+\Delta\alpha)z/\cos\theta}\left\{\sin^2\left(\frac{\pi z}{\lambda\cos\theta}\Delta n_o\right)+\sinh^2\left(\frac{z}{4\cos\theta}\Delta\alpha_o\right)\right\} \qquad [3.7]$$

where Δn and $\Delta\alpha$ are related to the free electrons through σ and σ_n, respectively. Any time dependence of the scattering enters the equation through the time dependence of the free carriers. This is determined by the diffusion equation[30]:

$$\frac{\partial N}{\partial t} = -\frac{N}{\tau} + \nabla(D\nabla N)) \qquad [3.8]$$

where, in general, the lifetime, τ, and the diffusion coefficient, D, are carrier concentration dependent. Using the results of the previous section, carrier concentrations generated by the write beams are expected to be small enough to ignore these higher order terms. However, for the sake of completeness, these terms were included.

Figure 3.4 shows the scattering efficiency of the probe beam as a function of the delay and the pump beam energy for CdTe. There are two interesting time regimes to be considered, (i) delay=0 and (ii) delay>0. In the first case, we see that the scattering efficiency increases with the pump beam energy followed by saturation and a subsequent decrease in the scattered signal. This behavior is typical for scattering from a phase grating (first term in Eq. 3.7). In a highly degenerate semiconductor, however, the contributions may oppose those due to a pure phase grating[30]. To elucidate the significance of the absorption grating, using the results of the preceding section, carrier concentrations in the peaks of the grating were determined for these regions. At these levels any contribution from the absorption grating can be neglected. A fit to the zero delay efficiency confirmed this result as well as yielding a value of 2.6 for the magnitude of σ_n in excellent agreement with the value found earlier.

Figure 3.5 is a plot of the time dependence of the scattering efficiency for a number of pump generated carrier concentrations. From Eq. 3.8, an exponential decay of the grating is

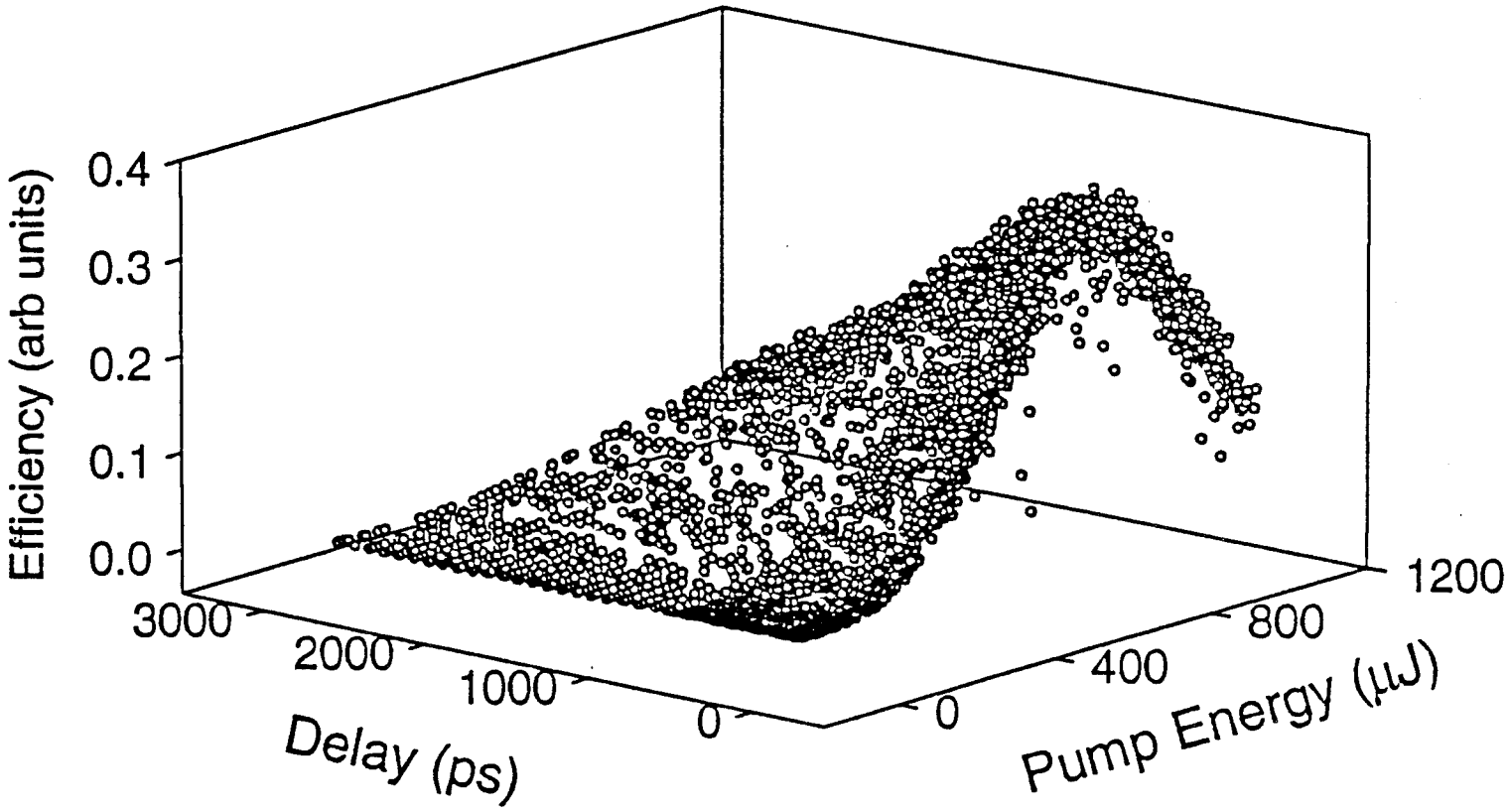

Fig. 3.4. Scattering efficiency of the probe beam as a function of the pump beam energy and probe beam delay.

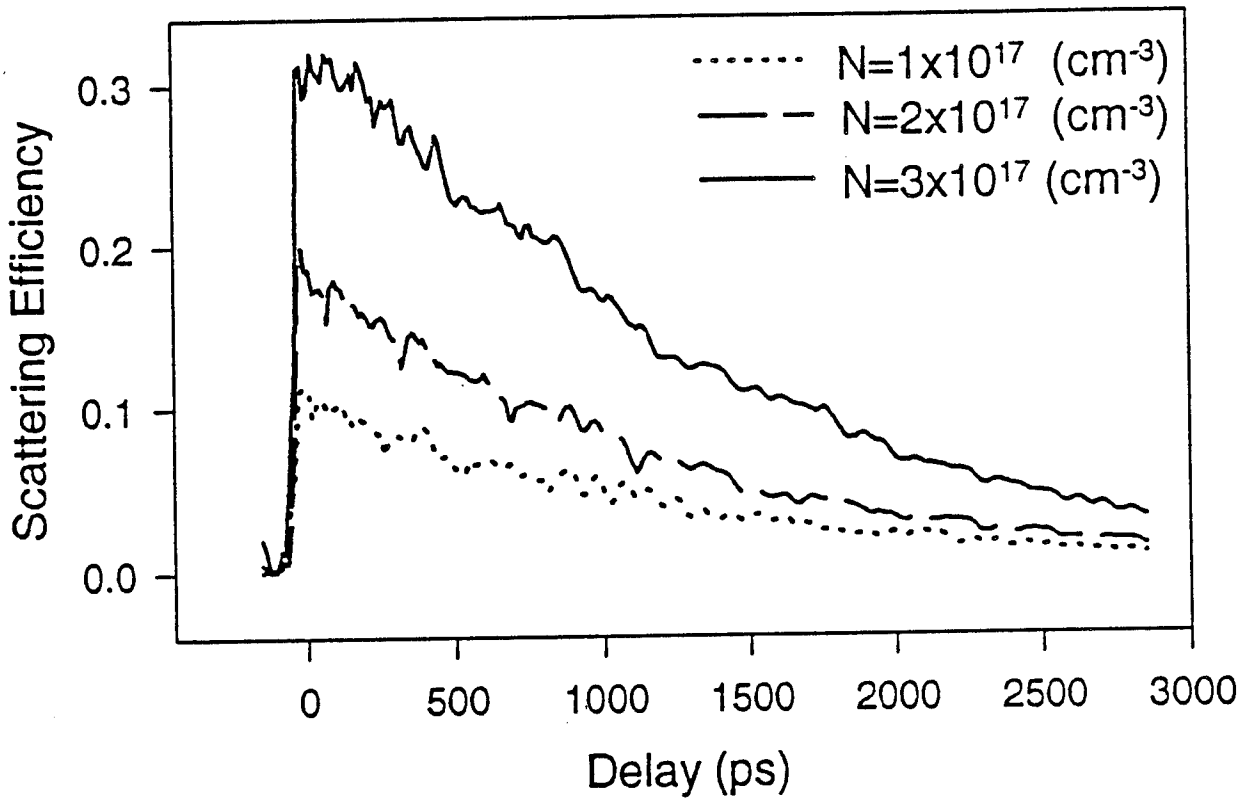

Fig. 3.5. Scattering efficiency of the probe beam as a function of the delay for a number of pump generated carrier concentrations.

expected with the decay time, τ_g, dictated by the recombination lifetime of the carriers and the ambipolar diffusion coefficient[10]. Substitution of this result into Eq. 3.7 predicts a time dependence for the scattering efficiency of the form $\eta(t) \sim \sin^2(a \exp(-t/\tau_g))$. For small values of a, this reduces to the familiar exponential decay. This is in accordance with the observed time behavior presented in Fig. 3.5.

It is possible to determine the recombination life time of the carriers from the time dependence of the total probe beam energy emerging from the sample. From Eq. 3.7, we see that attenuation of the probe beam can occur by (i) scattering in the Bragg direction and (ii) absorption by the carriers. The latter will be present for the scattered beam also, and is insensitive to the spatial nature of the carrier concentration. Furthermore, this absorption persists throughout the duration that the electrons are in the conduction band. Therefore, by monitoring the total energy of the post sample probe beam, scattered+transmitted, as a function of time, it is possible to determine the carrier lifetime. Figure 3.6 shows the total probe energy after the sample vs. time for different carrier concentrations. The time dependence of the signal has no saturation effects. This further emphasizes that the saturation observed in the FWM scattering efficiency was not caused by a saturation in the generated free carriers. Figure 3.6 was used to determine the lifetime of the electrons in the band. It was found that for the concentrations reached, the decay, τ, was a constant.

3.4 SUMMARY

Table 3.1 is a summary of the measured parameters for each sample. There are a few points of interest. First, the two photon absorption, β, and the nonlinear refraction, γ,

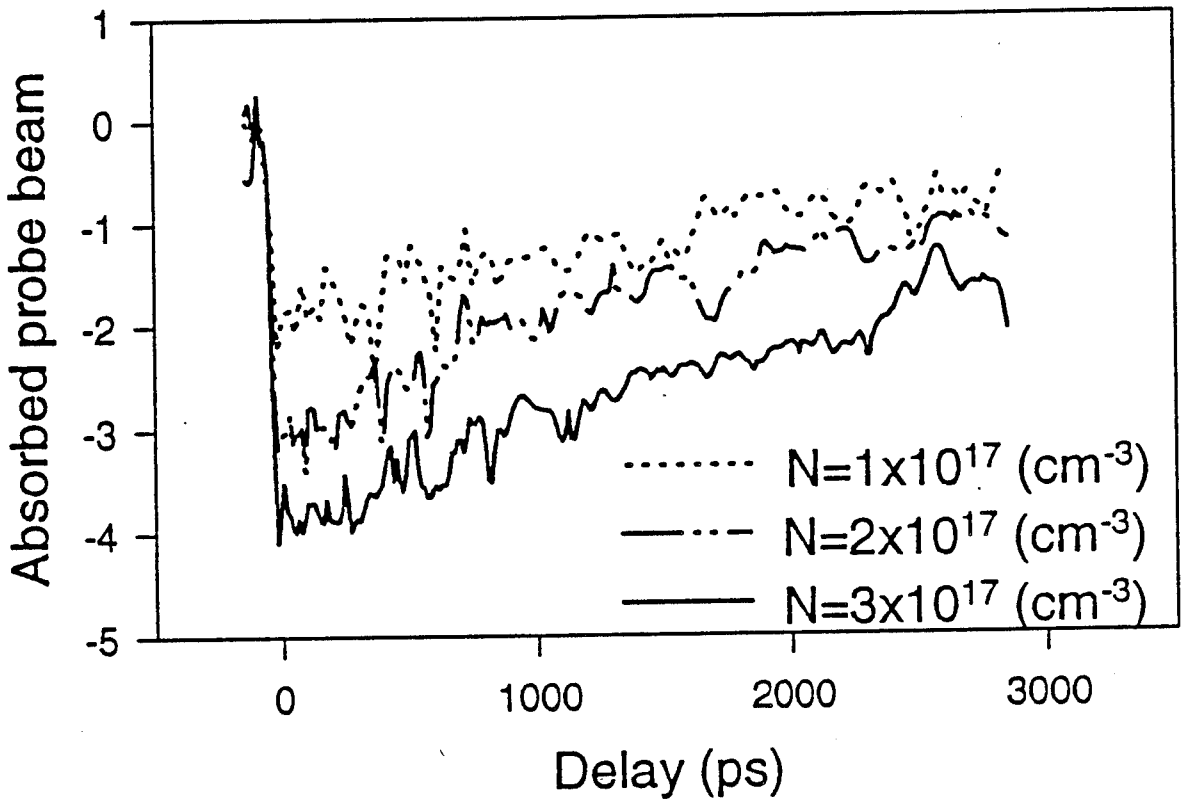

Fig. 3.6. Loss in the probe beam energy vs delay for different carrier concentrations.

coefficients decrease with an increase in the Mn concentration. This is to be expected, since addition of Mn will result in an increase in the band gap of the DMS, and these coefficients are inversely proportional to the band gap. Second, the free carrier absorption cross section remained constant for $Cd_{1-x}Mn_xSe$, but decreased for $Cd_{1-x}Mn_xTe$. The origin of this is not known, but it may be related to the strain present in $Cd_{1-x}Mn_xTe$ due to addition of Mn. Finally, the recombination lifetime of $Cd_{1-x}Mn_xSe$ increased with the Mn concentration with the exception of x=0.30 value, which may be due to presence of In in these samples. Furthermore, from the fits it was concluded that for the carrier concentrations achieved (10^{17} cm^{-3}), the concentration dependence of the recombination lifetime plays an insignificant role in the recombination process.

Table 3.1: Material parameters

Material	Thickness (mm)	$\beta(cm/GW)$	$\sigma(10^{-18}cm^2)$	$\sigma_{\tau o}(10^{-21}cm^3)$	$\tau(ns)$
CdSe	0.695	35	5	-2.7	4.4
$Cd_{0.9}Mn_{0.1}Se$	0.695	20	5	-1.5	7.0
$Cd_{0.8}Mn_{0.2}Se$	0.695	15	5	-2.0	12.0
$Cd_{0.7}Mn_{0.3}Se$:In	0.695	10	5	-1.1	2.2
$Cd_{0.6}Mn_{0.4}Se$	0.695	2.5	5	-0.6	71.4
CdTe	0.802	20	20	-2.5	4.8
$Cd_{0.9}Mn_{0.1}Te$	0.980	15	13	-2.5	*
$Cd_{0.6}Mn_{0.4}Te$	2.46	6.5	5	-0.75	*

* Signal insufficient for accurate determination

4. NONLINEAR OPTICAL RESPONSE OF SBN

4.1. INTRODUCTION

Strontium Barium Niobate ($Sr_xBa_{1-x}Nb_2O_6$), SBN: 100x, has been extensively studied for applications in optical storage and processing in the continuous wave (cw) laser regime[31-33]. Here we extend these investigations to include experiments that use short duration (picosecond and subpicosecond), high intensity laser pulses. The nonlinear optical responses to short laser pulses have previously been reported on photorefractive materials such as $Bi_{12}SiO_{20}$ [34,35,36,37,38,39,40], $Bi_{12}GeO_{20}$[40], $BaTiO_3$[41,42], $KNbO_3$[43], $LiNbO_3$[44], $KTa_xNb_{1-x}O_3$ [45], and Bi_2TeO_5[46] using nanosecond and picosecond pulses. The time scales for the electro-optic signals in these crystals range from less than 100 ps for $BaTiO_3$ up to 1 ms for $KNbO_3$.

For insulating crystals under low intensity, cw, visible light illumination, the donor and acceptor levels in the band gap of the material are important because they are the principal means for producing mobile charges. These band gap states are not the only mechanism for free carrier production in the short laser pulse regime. Direct band-to-band transitions become possible by multi-photon absorption when very intense light is used. This process produces an electron in the conduction band as well as a hole in the valence band, both of which are, in general, mobile. Most likely these 'extra' carriers will greatly affect the transient dynamics of any process that relies on free carrier production and motion, e.g. the photorefractive effect. The first part of this section discusses the measurement of the two photon absorption coefficient for our samples and the second part discusses four wave mixing (FWM) experiments.

SBN crystals are ferroelectric with an open tungsten-bronze structure. They display excellent nonlinear optical properties, in particular, they are an attractive photorefractive material because of their large r_{33} electro-optic coefficient. Additionally, SBN is one of only a handful of materials that exhibit self-pumped phase conjugation[33]. Material properties can be tailored by varying the crystal composition and by incorporating impurity ions at open lattice sites. The nominally undoped and iron-doped, optical quality $Sr_{0.60}Ba_{0.40}Nb_2O_6$ (SBN: 60) single crystals used in the experiments reported here were grown using the Czochralski technique. The iron concentration of the doped crystal was 0.012 weight percent; and it is expected that iron is present in both its Fe^{2+} and Fe^{3+} charge states. An automatic diameter control unit was used in the growth of the iron-doped sample to obtain striation free crystals. Individual samples were cut from the boule, optically polished, and completely poled to a single domain using fields less than 10 kV/cm[31]. The dimensions of the samples were 5.0x5.7x5.7 mm^3 and 5.9x6.1x6.1 mm^3 for the undoped and iron-doped respectively.

4.2. EXPERIMENT

The subpicosecond source used was the amplified output of a Spectra-Physics model 3500 synchronously pumped femtosecond dye laser. The pump source for the dye laser was a Spectra-Physics model 3800 cw, mode-locked Nd:YAG laser whose pulses were compressed via the standard optical fiber/grating pair method and then frequency doubled to 532 nm. The 580 nm, 350-450 fsec duration dye laser pulses were then amplified by a three stage pulsed dye amplifier (PDA). The PDA was pumped by an injection seeded, Q-switched Spectra-Physics model GCR-3 Nd: YAG laser. Single high energy subpicosecond pulses were obtained by

operating the amplifier in its single shot mode. For the picosecond laser studies the source was the frequency doubled output of a Continuum model YG571C Q-switched and mode locked Nd: YAG laser producing single 20 ps pulses at 10 Hz. An individual pulse was then separated using a mechanical shutter.

In the experiment to determine the two photon absorption (TPA) coefficient, single laser pulses were passed through the sample and the energy transmission coefficient was measured as a function of incident pulse energy. The incident energy was varied using a polarizing beam splitter preceded by a polarization rotator. The polarization was maintained such that it was the same as a write pulse in the FWM experiments described below, perpendicular to the c-axis of the crystal. The incident and transmitted laser pulse energies were measured with a Laser Precision model Rm-6600 universal radiometer with two model RJP-735 probes.

In the FWM experiment a single pulse was split into two parts of equal energy (hereafter referred to as 'write' pulses) which were focused such that they overlapped spatially and temporally in the sample ideally producing a spatially harmonic interference pattern. The angle between the paths of the pulses was 3.2 degrees measured in the air. A low power, cw He-Ne laser aligned at the Bragg angle for maximum diffraction from the grating was also focused in the sample. The beam geometry and crystal orientation was the usual photorefractive configuration used for FWM studies in SBN[47], i.e. the π-polarized He-Ne laser beam was crossed in the sample with the two σ-polarized write beams which were oriented with respect to the crystal such that they produced a grating wavevector that was parallel to the c-axis (see Fig. 4.1). To improve the signal-to-noise ratio, the probe beam propagation direction was aligned

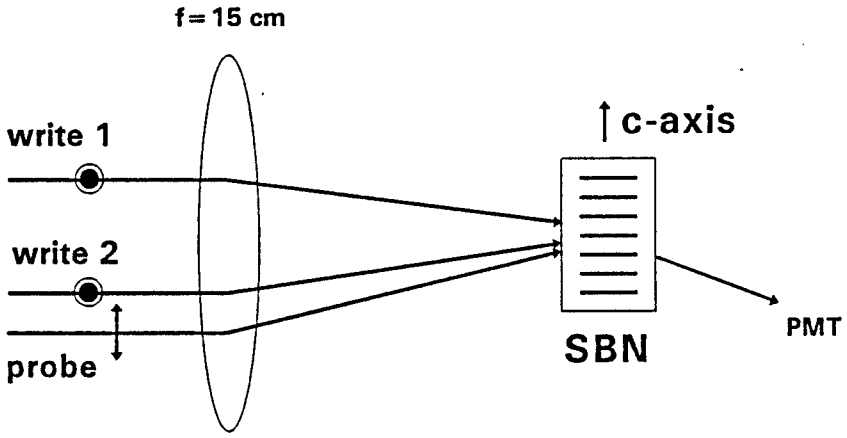

Fig. 4.1. Beam geometry for FWM experiments. π-polarized cw He-Ne probe beam, and σ-polarized subpicosecond (λ=580 nm) or picosecond (λ=532 nm) write pulses.

out of the plane containing the write pulses. The diffracted beam was detected using a photomultiplier tube with a rise time of approximately 2 ns and a digital storage oscilloscope. An interference filter at the He-Ne laser wavelength was used to ensure that no stray light from the pulsed laser entered the photomultiplier tube.

4.2.1. Two Photon Absorption

The differential equation describing the intensity (I) depletion of electromagnetic wave after a length z in an isotropic material is[48]

$$\frac{dI}{dz} = -\alpha I - \beta I^2 \qquad [4.1]$$

if only I and I^2 dependencies are assumed. In Eq. 4.1, α is the linear absorption coefficient and β is the TPA coefficient. In general the transmission of an intense laser pulse can be reduced in a number of other ways. Single photon absorption by free carriers produced by the pulse can lend an important contribution to the reduction. This is not accounted for in Eq. 4.1. Using the subpicosecond laser system we have eliminated the possibility of significant contribution from this effect by passing a weak probe pulse through the sample 2 ps being the original strong one. The probe was a split component of the strong pulse and 1000 times less intense. A mechanical delay line was used to obtain the 2 ps time difference. If there were free carrier absorption, the probe pulse would have been attenuated increasingly as the strong pulse energy is increased. Transmitted probe pulse energies were recorded as a function of incident strong pulse energies. The numbers were compared with the probe transmission recorded when the strong pulse was

blocked from entering the sample. Except for small *increase* in transmission of the probe pulse at the lower energies, its transmission was unaffected by the presence of the strong pulse. This result supports, to a good approximation, the exclusion of single photon free carrier absorption in our calculation of β. The increased being at low pump pulse energies could be due to an initial saturation of the linear absorption.

We note that single photon absorption following second harmonic generation (SHG) can also lend an important contribution to the TPA coefficient because the second harmonic of 532 nm and 580 nm both lie well within the intrinsic absorption range of SBN:60 and Fe:SBN:60. However, this effect is thought to be negligible in this case because SHG relies heavily on the phase matching condition which is not satisfied in the experiments reported here.

For beam propagation in the z-coordinate direction, the solution of Eq. 4.1 has the following form.

$$I(x,y,z,t) = \frac{I(x,y,0,t)e^{-\alpha z}}{1+\frac{\beta}{\alpha}I(x,y,0,t)(1-e^{-\alpha z})} \qquad [4.2]$$

A single reflection from the front and back surface can easily be included the obtain

$$I(x,y,z,t) = \frac{(1-R)^2 I(x,y,0,t)e^{-\alpha z}}{1+\frac{\beta}{\alpha}(1-R)I(x,y,0,t)(1-e^{-\alpha z})} \qquad [4.3]$$

where R is the reflection coefficient.

The spatial profile of the picosecond laser source was determined using a 15 micron pinhole and a photodiode. A Gaussian fit to this data was performed yielding a e^{-1} radius of

r_0=0.061 cm. A gaussian temporal profile was also used and was taken to have a half width of τ=13 ps at the e^{-1} point.

With the spatial and temporal profiles as described above the transmitted intensity can be written [49]

$$T = \frac{(1-R)^2 I_o e^{-(r/r_0)^2} e^{-(t/\tau)^2} e^{-\alpha z}}{1 + \frac{\beta}{\alpha}(1-R) I_o e^{-(r/r_0)^2} e^{-(t/\tau)^2} (1 - e^{-\alpha z})} \qquad [4.4]$$

where I_o is the maximum intensity of the pulse, $I_o = E_o/(\pi^{3/2} r^2 \tau)$.

The energy transmission coefficient through a sample of length l is then given by

$$T = \frac{2\alpha e^{-\alpha l}}{\beta I_o \sqrt{\pi}\,(1 - e^{-\alpha l})} \int_0^\infty \ln\left[1 + \frac{\beta}{\alpha} I_o (1-R)(1 - e^{-\alpha l}) e^{-x^2}\right] dx \qquad [4.5]$$

A value for the reflection coefficient was calculated by using the published value for the index of refraction of SBN:60[51]. This value was confirmed to be valid for our samples by a simple Brewster's angle experiment and calculation. The resulting value for the intensity reflection coefficient is R=0.16.

The energy transmission coefficient was measured by passing a single 22 ps pulse through a sample while monitoring both the incident and transmitted energies. Data were collected for a range of incident energies and the results for the undoped and iron-doped samples are plotted in Fig. 4.2. Eq. 4.5 was fit to this data using the commercial program Mathematica while allowing β to vary as free parameter. α was also allowed to vary in the fit but its value

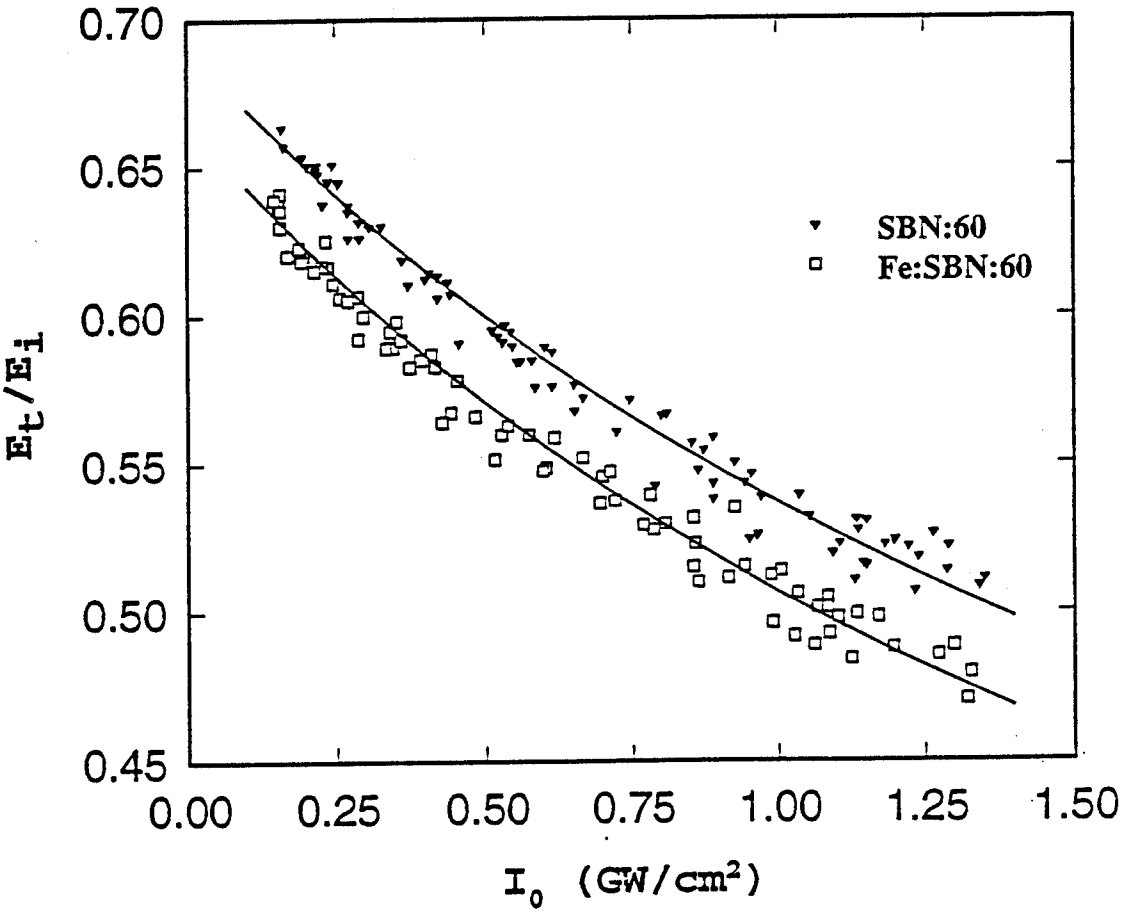

Fig. 4.2. Picosecond pulse energy transmission coefficient versus maximum incident intensity.

was restricted to 10% of the value determined using a Cary 2400 spectrophotometer. The solid line in the figure represents the results of the fitting procedure. The parameters for the undoped sample were $\alpha = 0.05$ cm^{-1} and β=2.3 cm/GW, and for the Fe-doped sample they were α=0.1 cm^{-1} and β= 2.15 cm/GW.

The same experiment was performed on the undoped sample using the subpicosecond laser system operating at a wavelength of 580 nm. The spatial and temporal profiles of the pulses were such that they were best modeled as uniform (crossectional area=3.14x10^{-2} cm^2) and gaussian (half width at e^{-1}, τ=240 fs) respectively. This results in a functional change in the energy transmission coefficient,

$$T = \frac{(1-R)^2 e^{-\alpha l}}{\sqrt{\pi}\,\tau} \int_{-\infty}^{\infty} \frac{dt}{e^{(t/\tau)^2} + \frac{\beta}{\alpha} I_o (1-R)(1-e^{-\alpha l}} \qquad [4.6]$$

where Io has the same functional form, $I_o = E_o/(\pi^{3/2} r^2 \tau)$.

Figure 4.3 is a plot of transmission coefficient versus incident intensity for the experiment using the subpicosecond laser source. The solid line represents a fit of Eq. 4.6 to the data where, once again, β is a free parameter. The resulting value for the TPA coefficient is 2 cm/GW, in reasonable agreement with that measured for the shorter wavelength of 532 nm.

4.2.2 FWM: Experimental Results

4.2.2.1. Picosecond-pulse excitation:

With excitation pulses of 20 ps duration and 532 nm wavelength there were two distinct temporal features seen in the FWM signal for both samples. Typical data obtained for the undoped sample are shown in Fig. 4.4. After the initial unresolved buildup the first decay of the

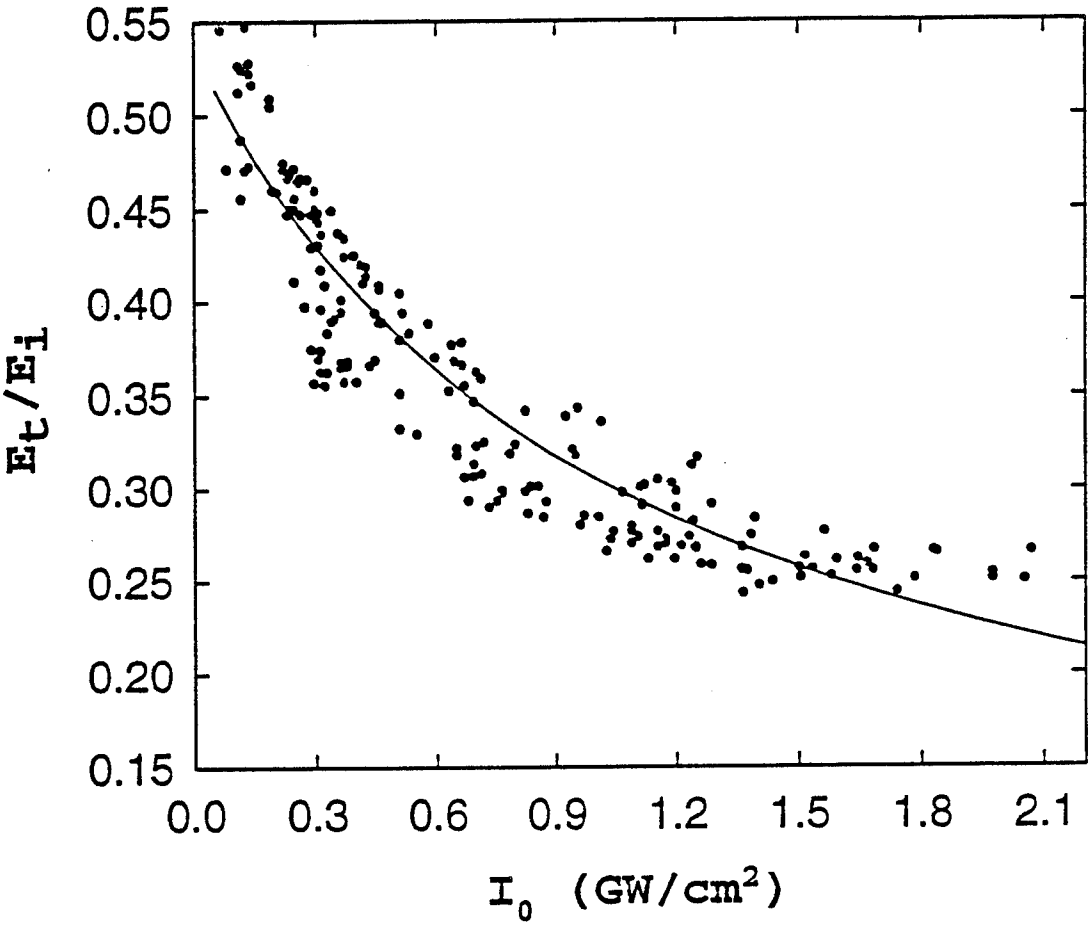

Fig. 4.3. Subpicosecond pulse energy transmission coefficient versus maximum incident intensity

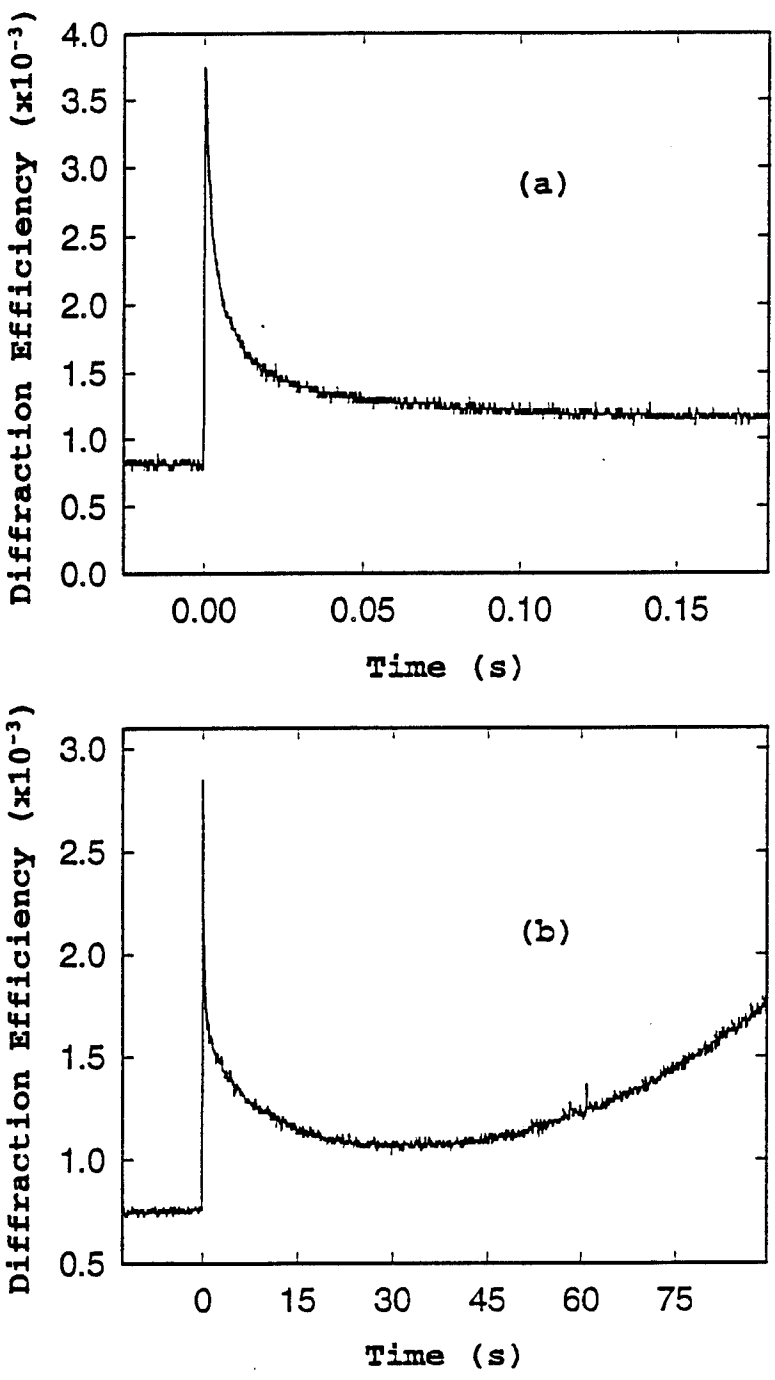

Fig. 4.4. FWM signal following picosecond excitation in SBN:60 with write beam incident energies of : (a) 47 μJ and (b) 46.4 μJ.

FWM signal is in the 100 ms time scale. This was followed by a comparatively slow rise that reaches its maximum after a few minutes (Fig. 4.4(b)). In the case of a total write beam energy of 78 μJ the second rise is complete in approximately four minutes and decays to half the peak height after another fifteen minutes.

Typical FWM data obtained using the Fe:SBN sample are shown in Fig. 4.5. Similar to the signal from the undoped sample, there exists two stages to the signal in the time frame studied, however the time scales associated with them are very different. The decay of the first signal is complete in less than 25 ms and is followed by a rise of the second signal that is complete in less than 20 seconds. For pulse energies lower than those shown in Figs. 4.5(a) and 4.5(b) e.g., Fig. 4.5(c), the detected signal is observed to drop below the background level in the time regime just after the first signal decay. This means that there must be a process that had decreased the total amount of background light that is randomly scattered from the sample to the detector. For both samples the cross-sectional area of interaction for the two write pulses was 2.7×10^{-5} cm^2.

4.2.2.2. Subpicosecond-pulsed excitation:

In a manner similar to that which was seen using the ps pulses, excitation using 400 fs, 580 nm pulses produces two temporal features to the diffracted signal in the time scale of interest in these experiments. Typical data for the undoped sample are show in Fig. 4.6. The first feature in Fig. 4.6(a) is a peak that has a rise time of 3000-600 ns which is time resolved in Fig. 4.6(b). The initial spike in the data seen in Fig. 4.6(b) is due to gratings formed on the time scale of the temporal overlap of the two write pulses and is not of interest in this work. This

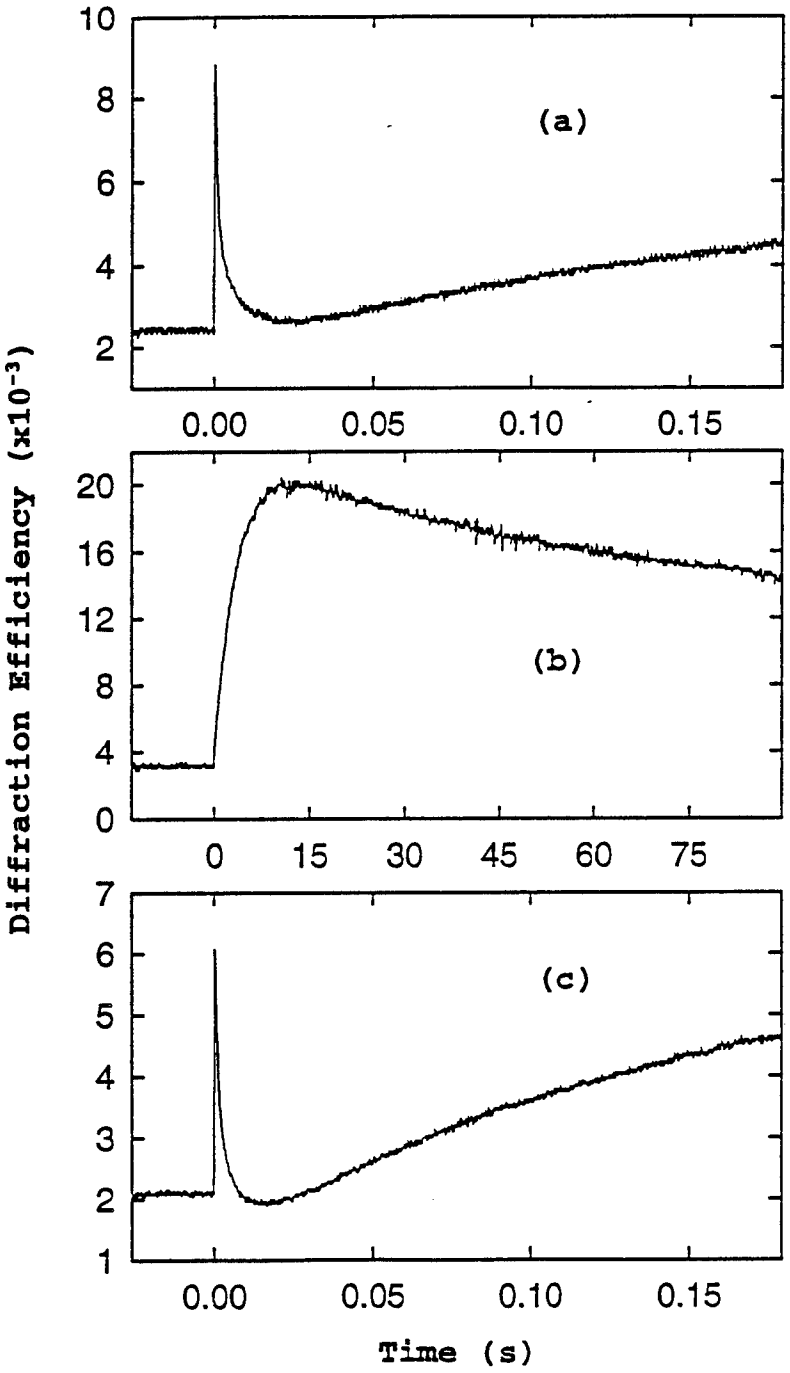

Fig.4.5. FWM signal following picosecond excitation in Fe:SBN:60 with write beam incident energies of : (a) 42.8 μJ , (b) 50 μJ, and (c) 18.5 μJ

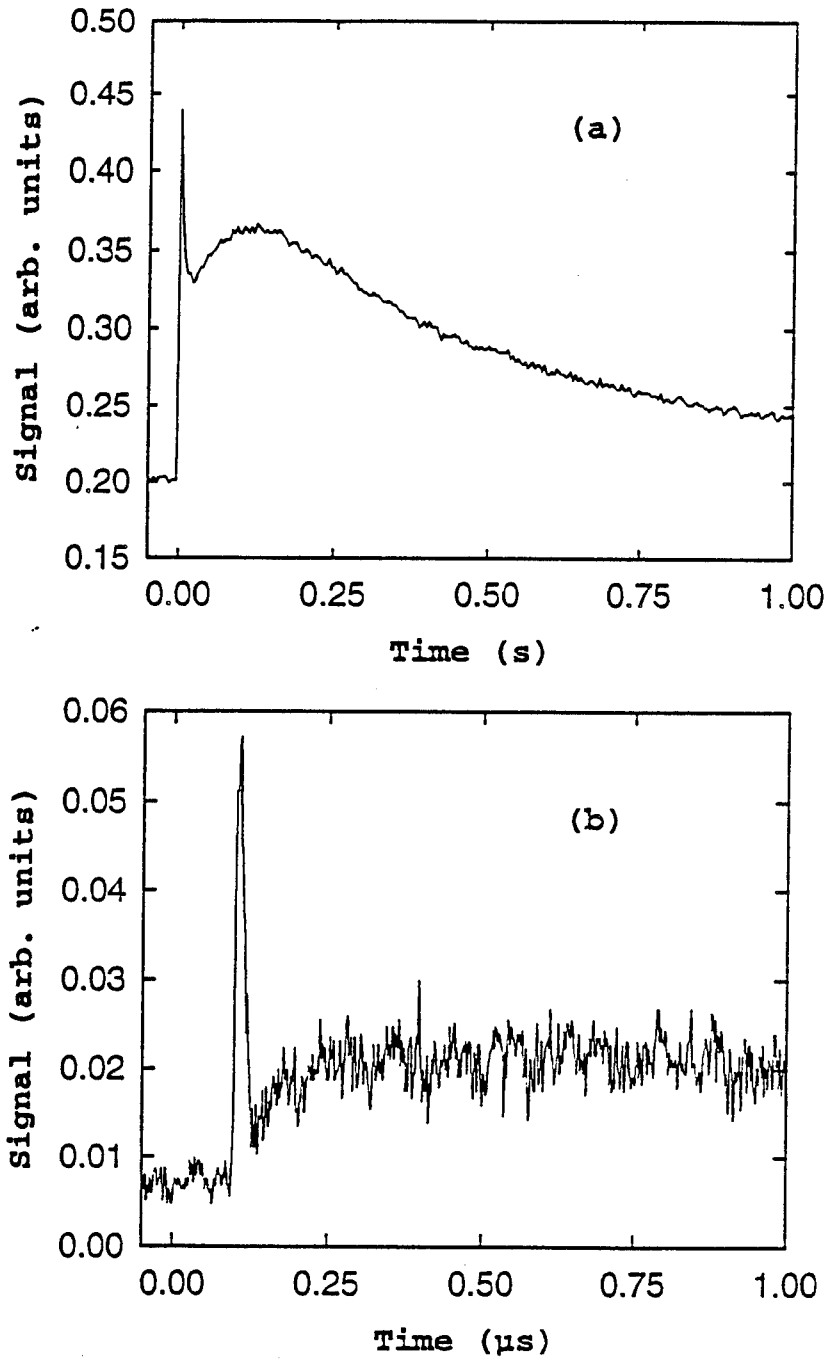

Fig. 4.6. FWM signal following subpicosecond excitation in SBN:60 in the time scale of (a) seconds and (b) microseconds.

signal decays into the microsecond time scale where it competes with the rise of the second signal. The time constants associated with the second peak depend strongly upon the intensity of the write pulses. It has been observed to last as long as thirty seconds or as short as few hundred milliseconds.

Experiments on the Fe-doped samples were not performed using the subpicosecond laser system.

4.2.3 Discussion:

4.2.3.1. Undoped sample:

The first signal in both the picosecond and subpicosecond experiments is associated with scattering from a grating that is set up by an optically induced absorption change in the bright regions for the interference pattern of the two write pulses. In order to demonstrate that intense light at both 580 nm and 532 nm induces absorption at 632.8 nm, one of the write pulses and the He-Ne laser were crossed in the sample, and the transmitted He-Ne laser beam was monitored with the same detection scheme as discussed above for FWM. The results of the experiment using the picosecond and subpicosecond laser are shown in Fig. 4.7(a) and 4.7(b), respectively. In both cases, the time dynamics of the induced absorption are the same as those of the first signal in the FWM experiments. It is interesting to note that the same type of probe beam depletion was observed using the green line (543 nm) of the He-Ne laser as the probe. The recovery of the transmission, however, was noticeably slower for the shorter wavelength. This suggests that the site(s) responsible for the 543 nm absorption have a longer lifetime. With the experiments described thus far it is not possible to determine the physical mechanisms responsible for the induced absorption. It is proposed that the induced absorption is a result of

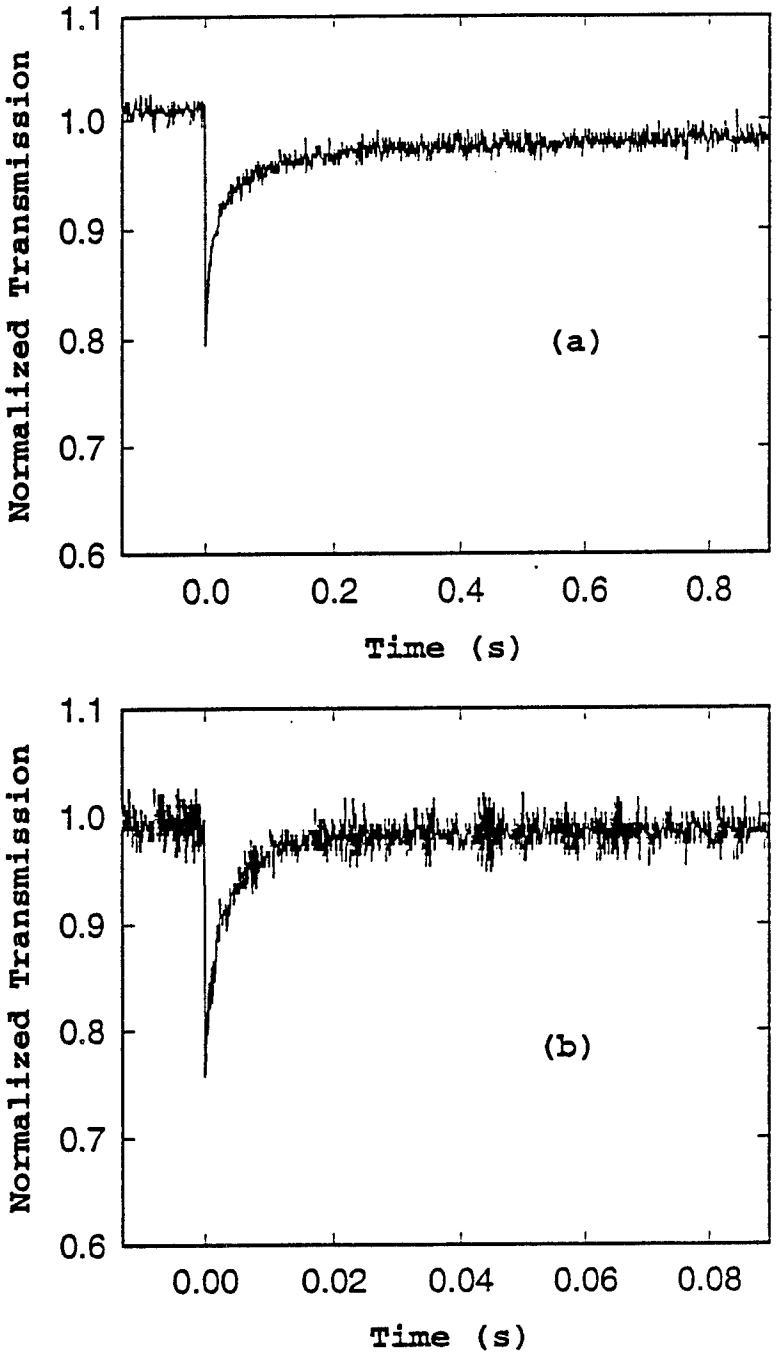

Fig. 4.7. Probe beam depletion following (a) 46.1μJ picosecond excitation and (b) 1.1 μJ subpicosecond excitation.

the population of impurity or defect site that did not have significant population before excitation. Further, it is thought that significant population of this level can only be realized with the aid of a larger number of two photon band-to-band transitions followed by trapping at the site(s) that absorb near 632 nm. The TPA coefficient at 532 nm, as discussed in the previous section, is 2.3 cm/GW. With an intensity of 2.5 GW/cm^2 the intensity depletion of a laser beam through undoped SBN:60 is more than an order of magnitude greater than that of the linear absorption. Below this value of intensity, the transient probe beam depletion becomes an unmeasurable effect without detection system, in SBN:60. After excitation the free carriers populate an absorbing level at a rate that is roughly inversely proportional to the rise time of the induced absorption. The decay of the grating is due to the depopulation of the absorbing level either through recombination of trapping at other site(s) that do not absorb at 632.8 nm.

The subsequent rise of the diffracted signal after the decay of the absorption grating is explained as due to the usual charge displacement photorefractive effect [19]. It can only be observed when the beam geometry is such that photorefractive effects are possible. At this time the mechanism of charge transport as well as the sign of the charge carrier is not apparent. In cw FWM experiments electrons have been found to be the dominant carrier[1]. However, competition from holes cannot be ignored in the pulsed regime because the direct band-to-band transitions that are associated with nonlinear absorption create a large number of holes. Their contribution to the grating depends on their relative mobility with respect to electrons.

4.2.3.2 Fe-doped sample:

The time scales of the two temporal features of the FWM signal in Fe:SBN are very different in comparison with the signal in the undoped sample. The first difference is seen in the

much faster decay followed by a drop in the signal below the background level for the lower energies studied. This effect is not observed at higher intensities because the rise of the second peak begins earlier for increasing intensities and competes with the decay of the first signal. Such a drop in the signal below background can be explained by an increased absorption at the probe wavelength which, once the first grating has decayed, reduces the amount of scattered light that passes through the sample to the detector. Since in our model the first signal is associated with induced absorption the faster decay of the first signal would suggest that the induced absorption would also decay faster. On the contrary, however, the induced absorption experiment in the Fe-doped sample showed that the depletion lasted longer. This can be seen in Fig. 4.8. This result indicates that the absorption grating is destroyed prior to the depopulation of the levels responsible for it. This suggests that the absorbing levels in the dark regions are populated on the time scale that is associated with the decay. Population of these levels reduces the contrast ratio of the grating and therefore the diffracted signal. Induced absorption is still present after the decay of the grating is complete because the absorbing levels are still populated. This reduces the background scatter at the detector. This effect is not observed in the undoped sample because it does not have the advantage of increased carrier mobility due to the iron dopants. This increased mobility as a result of iron doping is also responsible for the faster buildup of the photorefractive grating in this sample. As with the undoped sample, TPA is the dominant free carrier production mechanism in Fe:SBN.

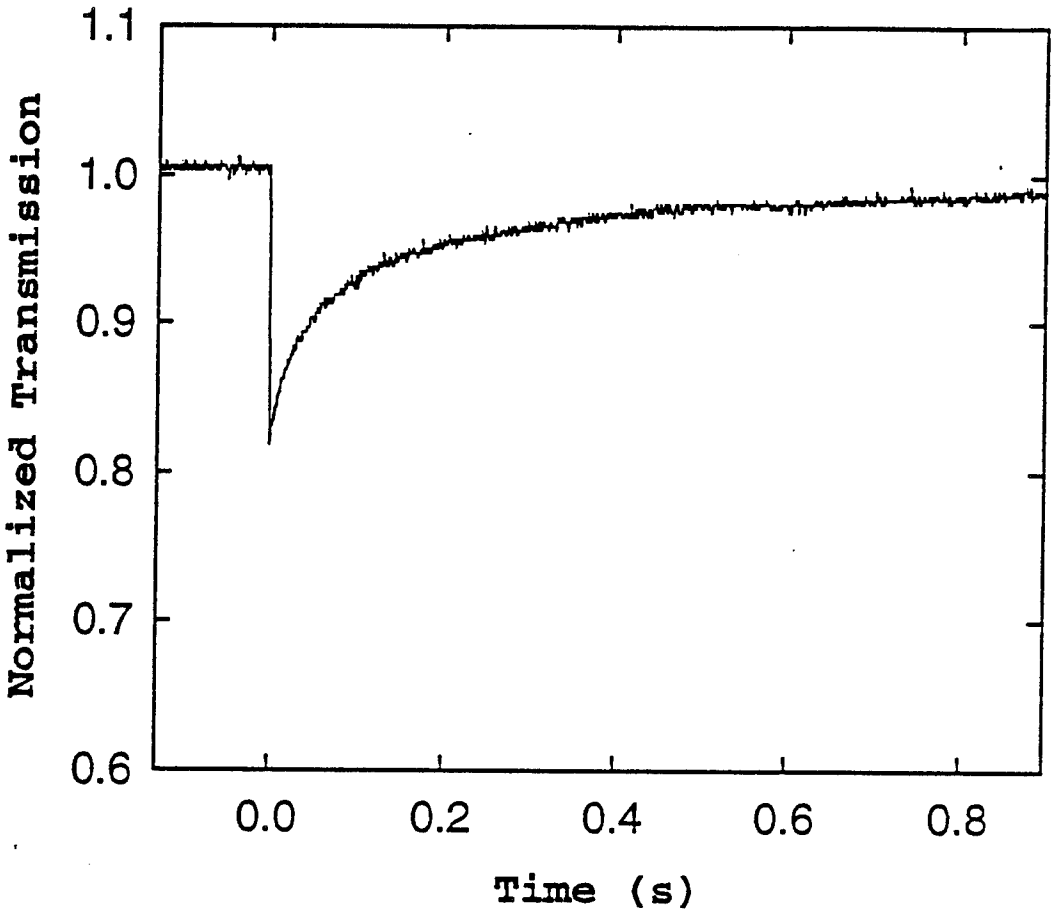

Fig. 4.8. Probe beam depletion following a 41.4 μJ picosecond excitation

4.3. CONCLUSIONS

Single picosecond and subpicosecond light pulses were used in independent experiments to induce refractive index gratings in SBN:60. The time evolutions of the gratings appear to have at least two stages which are responsible for two distinct peaks in the FWM signal. The first peak is associated with induced absorption at the probe wavelength. In a single beam experiment, where no grating was present, it was shown that significant probe beam depletion is seen following intense excitation. This depletion is explained as induced absorption due to the population of an impurity or defect site and is associated with the first peak in the FWM signal because the time scales of the two phenomena overlapped. The second peak is explained as resulting from a grating due to a charge displacement photorefractive effect. It can only be observed when the beam geometry is such that photorefractive effects are possible. The TPA coefficient of both samples was measured and the numerical values obtained indicate that TPA is the dominant free carrier production mechanism at the intensities used in these experiments.

5. SUMMARY AND RECOMMENDATION

We have looked at the nonlinear optical properties of lead galliate glasses, diluted magnetic semiconductors and strontium barium niobate photorefractive crystal for possible application as optical limiters. During the original work on potential materials for optical limiting, we demonstrated that for clamping levels required for eye protection some linear absorption was necessary. We also showed that lead based glasses have the greatest potential as materials capable of achieving this goal. Under nanosecond illumination, absorption of light led to local thermal changes in the material which in turn caused changes in the local refractive index and absorption coefficients. These changes were used to achieve optical limiting in an F/20 system. Using an F/5 system, we focused on lead galliates which showed the greatest promise among the lead based glasses. The low cost of production, ease of material tailoring and their durability makes these materials ideal for devices. Optical limiting was observed throughout the 440-640 nm spectral range for 7 ns laser pulses. Optical limiting was also observed for uniform and/or off-axis illumination. A minimum clamping level of 10 mJ/cm^2 for a 7 ns pulse at 457 nm was achieved which is slightly higher than the desired value. Lower clamping is attainable with an offset of further reduction in the linear transmission. In particular, the clamping level was found to be inversely related to the linear transmission of the sample. This, in addition to their low surface damage threshold, is the greatest shortcoming of these materials. Furthermore, since the physical process behind optical limiting is thermal, the material will not be useful against short pulse lasers.

It is well known that free carriers exhibit large nonlinear optical properties with ultrafast rise times. Therefore, in principle, it is possible to have a high damage threshold and a broad time

response in semiconductors. To overcome the difficulties observed in lead galliate glasses, a number of CdMnSe and CdMnTe samples were considered. The advantage of these materials over some other conventional semiconductors is the band gap tunablity due to presence of Mn ions. Using picosecond pulses from a Nd:YAG laser, the bulk carrier properties were investigated for different Mn concentrations. It was found that while the free carriers exhibited high degree of nonlinear optical behavior, the nonlinear refraction coefficient was carrier concentration dependent, saturating above a certain critical concentration. Furthermore, in the absence of significant trap levels, carrier generation could only be achieved via two photon absorption. This means that even though the linear transmission may be large, the threshold intensities needed to induce optical limiting would be too high for an efficient use of these materials as optical limiters. This is the main downfall of these materials. Increase in the number of trap levels may reduce the threshold intensity but will also result in a decrease in linear transmission. Even with addition of traps, these materials will lack broad band operation such as observed in the lead galliate glasses.

As an alternative material, we looked at strontium barium niobate photorefractive crystal. The advantages of photorefractive materials over the other two classes are that photorefractive crystal have a high damage threshold, a high nonlinear optical coefficient, and a broad time response. Carrier generation in these materials is achieved via single photon absorption of electrons from the defect levels or by two photon absorption from the valence band. The two photon absorption coefficient of most crystals is too small, resulting in similar problem as observed in semiconductors. The linear absorption, on the other hand, has a broader band in the visible region than semiconductors. However, this absorption is determined by the number of traps and as such is not very large. This means that, as with semiconductors, the efficiency of these materials as optical

limiters in the nanosecond time regime is much less than that of the glasses. Photorefractive crystals may prove useful for a narrow line optical limiting were significant defects levels are available.

In conclusion, the above results indicate that broad band optical limiting is possible in the nanosecond time regimes with proper material as the nonlinear medium. It seems that the achievable clamping level is offset by the acceptable linear transmission through the material. Glasses seem to be the best suited material due to their broad band response and ease of tailoring. We have looked at a number of different glasses for this purpose, but the possibilities have not been exhausted. Focusing on glasses, future research should include other hosts as well as other modifiers. Recently, C_{60} in toluene as possible active element in optical limiters has become popular. These materials have a narrower band than glasses but seem to demonstrate a high nonlinear optical behavior. Incorporation of C_{60} in a glass structure may prove a viable approach to this problem. Since intra C_{60} transitions may still be available, the material may also work in the short pulse regime.

6. REFERENCES

[1] E.P. Reidel and G.D. Baldwin, *J. Appl. Phys.*, **38**, 2720 (1967).

[2] M. Sparks, *J. Appl Phys.*, **42**, 5029 (1971).

[3] S.A. Akhmanov, R.V. Khokhlov and A.P. Sukhorrukov, *"Self-focusing, Self-defocusing and Self-Modulation of Laser Beams", in Laser Handbook,* (North-Holland, Amsterdam, 1972).

[4] J.H. Marburger, *Prog. Quantum Electron.*, **4**, 35 (1975).

[5] A.J. Twarowski and D.S. Kliger, *Chem. Phys.*, **20**, 253 (1977).

[6] J.P. Gordon, R.C. Leite, R.S. Moore, S.P.S. Porto and J.R. Whinnery, *J. Appl. Phys.*, **36**, 3 (1965).

[7] G.D. Baldwin and E.P. Riedel, *J. Appl. Phys.*, **38**, 2728 (1967).

[8] F.W. Dabby and J.R. Whinnery, *Appl. Phys. Lett.*, **13**, 284 (1968).

[9] A. Feldman, D. Horowitz and R.M. Walker, *IEEE J. Quantum Electron.*, **QE-9**, 1054 (1973).

[10] A.J. Twarowski and D.S. Kliger, *Chem. Phys.*, **20**, 259 (1977).

[11] G.L.Wood, W.W. Clark III, M.J. Miller, G.J. Salamo and E.J. Sharp, *SPIE,* **1105**, 154 (1989).

[12] G.L. Wood, W.W. Clark III and E.J. Sharp, *SPIE,* **1307**, 376 (1990).

[13] B. Taheri, A.F. Munoz, W.D. St. John, J.P. Wicksted, R.C. Powell, D.H. Blackburn and D.C. Cranmer, *J. Appl. Phys.*, **71**, 3693 (1992).

[14] B. Taheri, Masters Thesis, Oklahoma State Unviersity, 1991.

[15] R. Adair, L.L. Chase and S.A. Payne, *J. Opt. Soc. Am.*, **B4**, 875 (1987).

[16] M. Sheik-Bahae, A.A. Said and E.W. VanStryland, *Opt. Lett.*, **14**, 955 (1989).

[17] W.H. Dumbaugh, *Phys. Chem. Glasses,* **27**, 119 (1986).

[18] J.E. Shelby, *J. Am. Ceram. Soc.*, **71**, C-254 (1988).

[19] M. Sheik-Bahae, A.A. Said, D.J. Hagan, M.J. Soileau and E.W. VanStryland, *Opt. Eng.*, **30**, 1228 (1990).

[20] J.M. Jewell and J.A. Ruller, *J. Non-Cryst. Sol.*, to be published.

[21] J.K. Furdyna, *J. Appl. Phys.*, **64**, R29 (1988).

[22] See for example, *"Semiconductors and Semimetals"*, R.K. Willardson and A.C. Beer, Treatise Editors; J.K. Furdyna and J. Kossut, Volume Editors, (Academic, Boston, 1988), vol. **25.**

[23] E.W. Van Srtyland, H. Vanherzeele, M.A. Woodall, M.J. Soileau, A.L. Smirl, S Guha and T.F. Boggess, *Optical Engineering,* **24**, 613 (1985).

[24] M. Sheik-Bahae, D.C. Hutching, D.J. Hagan and E.W. Van Stryland, *IEEE J. Quantum Electron,* **27**, 1296 (1991).

[25] D. Weaire, B.S. Wherrett, D.A.B. Miller, and S.D. Smith, *Opt. Lett.*, **4**, 331 (1974).

[26] M. Born and E. Wolf, *"Principles of Optics"*, (Pergamon Press, Oxford, 1980).

[27] W. Zawadzki in *"Handbook on Semiconductors, vol 1: Band Theory and Transport Properties"*, T.S. Moss and W. Paul, Editors, (North Holland, Amsterdam, 1980).

[28] K.W. Boer, *"Survey of Semiconductor Physics"*, (Van Nostrand Reinhold, New York, 1990).

[29] H.J. Eichler, P. Gunter and D.W. Pohl, *"Laser-Induced Dynamic Gratings"*, (Springer-Verlag, New York, 1986).

[30] H.J. Eichler, F. Massmann, *J. Appl. Phys.*, **53**, 3237 (1982).

[31] M.D. Ewbank, R.R. Neurgaonkar, W.K. Cory, and J. Feinberg, *J. Appl. Phys.*, **62**, 374 (1987).

[32] D.Rytz, B.A. Wechsler, R.N. Schwartz, C.C. Nelson, C.D.Brandle, A.J. Valentino, and G.W. Berkstresser, *J. Appl. Phys.*, **66,** 1920 (1989).
[33] G. Samlamo, M.J. Miller, W. W. Clark III, G. L. Wood, and E. J. Sharp, *Opt. Comm.*, **59**, 417 (1986).
[34] G. Le Saux and A. Brun, *IEEE J. Quantum Electron.*, **QE-23**, 1680 (1987).
[35] D.C. Jones and L. Solymar, *Opt. Comm.*, **85**, 372 (1991).
[36] J. M. C. Jonathan, G. Roosen, and Ph. Roussignal, *Opt. Lett.*, **13**, 224 (1988).
[37] G. Le Saux, G. Roosen, and A. Brun, *Opt. Comm.*, **56**, 374 (1986).
[38] J.P. Hermann, J.P. Herriau, and J.P. Huignard, *Appl. Opt.*, **20**, 2173 (1981).
[39] J.-L. Ferrier, J. Gazengel, X.N. Phu, and G. Rivoire, *Opt. Comm.*, **58**, 343 (1986).
[40] G. Le Saux, J.C. Launay, and A. Brun, *Opt. Comm.*, **57**, 166 (1986).
[41] A. Smirl, K. Bohner, G.C. Valley, R.A. Mullen, and T. Boggess, *J. Opt. Soc. Am.*, **B6,** 606 (1989).
[42] L. Lam, T.Y. Chang, J. Feinberg, and R. Hellwarth, *Opt. Lett.*, **6**, 475 (1981).
[43] I. Biaggio, M. Zqonik, and P. Gunter, *Opt. Comm.*, **77**, 312 (1990).
[44] C.-T. Chen, D. Kin, and D. von der Linde, *IEEE J. Quantum Electron.*, **QE-16**, 126 (1980).
[45] R.J. Reeves, H. Liu, and R.C. Powell, to be published in *Phy. Rev. B.*
[46] I. Foldvari, B. Taheri, R.J. Reeves, and R.C. Powell, *Opt. Comm.*, **102**, 245 (1993).
[47] J.B. Thaxter and M. Kestigian, *Appl. Opt.*, **13**, 913 (1974).
[48] Y.P. Kim and M.H.R. Huchinson, *Appl. Phys. B*, **49**, 469 (1989).
[49] T.J. Hall, R. Jaura, L.M. Connors, and P.D. Foote, *Prog. Quant. Electr.*, **10**, 77 (1985).
[50] J.H. Bechtel and W.L. Smith, *Phys. Rev. B,* **13**, 3515 (1976).
[51] G.L. Wood, W.W. Clark III, M.J. Miller, E.J. Sharp, G. Salamo, and R.R. Neurgaonkar, *IEEE J. Quantum Electron.*, **QE- 22**, 2126 (1987).

6. PUBLICATIONS

[1] R.R. Petrin, A. Munoz F., R.J. Reeves, R.C. Powell, and J.M. Jewell
[2] B.Taheri, A. Munoz F., R.C. Powell, J.J. Song and J.K. Furdyna, *SPIE*, **2229**, 24(1994).
[3] S.A. Holmstrom, B. Taheri, R.J. Reeves, R.C. Powell, E.J. Sharp, and R.R. Neurgoankar, Submitted to Optics communication.
[5] Masters Thesis, S.A. Holmstrom, Dec. 1993.
[6] Doctoral Thesis, B. Taheri, Aug. 1994.